

1 **High throughput single-cell genome sequencing gives insights into the generation and**  
2 **evolution of mosaic aneuploidy in *Leishmania donovani***

3

4 Gabriel H. Negreira<sup>1</sup>, Pieter Monsieurs<sup>1</sup>, Hideo Imamura<sup>1</sup>, Ilse Maes<sup>1</sup>, Nada Kuk<sup>2</sup>, Akila Yagoubat<sup>2</sup>, Frederik  
5 Van den Broeck<sup>1,3</sup>, Yvon Sterkers<sup>2</sup>, Jean-Claude Dujardin<sup>1,4</sup>, Małgorzata A. Domagalska<sup>1</sup>

6

7 Authors Affiliation:

8 <sup>1</sup> Molecular Parasitology Unit, Institute of Tropical Medicine, Antwerp, Belgium

9 <sup>2</sup> MiVEGEC, University of Montpellier, CNRS, IRD, Montpellier, France

10 <sup>3</sup> Department of Microbiology, Immunology and Transplantation, Rega Institute for Medical  
11 Research, Katholieke Universiteit Leuven, 3000 Leuven, Belgium

12 <sup>4</sup> Department of Biomedical Sciences, University of Antwerp, Belgium.

13

14 Keywords: *Leishmania*, single-cell genomics, mosaic aneuploidy

15

16

17

**Note to the BioRxiv community:**

The present preprint is a revision of an older preprint posted on 06<sup>th</sup> March 2020 on BioRxiv (<https://www.biorxiv.org/content/10.1101/2020.03.05.976233v1>). Here we included two extra samples in our single-cell genome sequencing (SCGS) analysis – the BPK081 cl8 clone (a nearly euploid strain) and a population consisting of a mixture of four *L. donovani* strains which was used as control for high levels of mosaicism in aneuploidy and for estimation of doublets. We also upgraded the bioinformatics pipeline to determine single-cell karyotypes and performed new fluorescence in situ hybridization (FISH) analysis. The new findings observed especially in the BPK081 cl8 led to a reformulation of the text, a new hypothesis for the evolution of mosaicism and a general restructuring of the article. Therefore, the older preprint is obsolete.

18 **Abstract**

19 *Leishmania*, a unicellular eukaryotic parasite, is a unique model for aneuploidy and cellular  
20 heterogeneity, along with their potential role in adaptation to environmental stresses. Somy  
21 variation within clonal populations was previously explored in a small subset of chromosomes  
22 using fluorescence hybridization methods. This phenomenon, termed mosaic aneuploidy (MA),  
23 might have important evolutionary and functional implications but remains under-explored due  
24 to technological limitations. Here, we applied and validated a high throughput single-cell  
25 genome sequencing method to study for the first time the extent and dynamics of whole  
26 karyotype heterogeneity in two *Leishmania* clonal populations representing different stages of  
27 MA evolution in vitro. We found that drastic changes in karyotypes quickly emerge in a  
28 population stemming from an almost euploid founder cell. This possibly involves  
29 polyploidization/hybridization at an early stage of population expansion, followed by assorted  
30 ploidy reduction. During further stages of expansion, MA increases by moderate and gradual  
31 karyotypic alterations. MA usually affected a defined subset of chromosomes, of which some  
32 display an enrichment in snoRNA genes which could represent an adaptative benefit to the  
33 amplification of these chromosomes. Our data provide the first complete characterization of  
34 MA in *Leishmania* and pave the way for further functional studies.

35  
36

37 **Introduction**

38 Aneuploidy, i.e., an imbalance in the copy number of chromosomes in a cell, occurs in a  
39 wide range of organisms, including both non- and pathogenic unicellular eukaryotes, such as  
40 *Saccharomyces cerevisiae*, *Candida albicans*, *Cryptococcus neoformans* and *Leishmania* spp, but  
41 also in different types of human cancer cells (Downing et al., 2011; Holland and Cleveland, 2009;  
42 Mulla et al., 2014; Rogers et al., 2011; Selmecki et al., 2006; Sterkers et al., 2011). Although  
43 generally considered to be detrimental in multicellular organisms, aneuploidy can also be  
44 beneficial, in particular for unicellular organisms facing drastic changes in the environment  
45 (Gilchrist and Stelkens, 2019; Siegel and Amon, 2012). In pathogens, aneuploidy facilitates rapid  
46 adaptation to environmental stresses through changes in gene dosage and may have an impact  
47 on both virulence and the development of drug resistance (Beach et al., 2017; Gerstein et al.,  
48 2015; Gilchrist and Stelkens, 2019; Hirakawa et al., 2017; Hu et al., 2011; Ni et al., 2013; Reis-  
49 Cunha et al., 2017).

50 *Leishmania*, a genus of digenetic protozoan parasites, is emerging as a unique model for  
51 aneuploidy (Mannaert et al., 2012). These parasites are responsible for a spectrum of clinical  
52 forms of leishmaniasis worldwide and cause 300,000 new cases per year (WHO, 2020). They  
53 can be found in two forms during their life cycle: as an extracellular promastigote in the midgut  
54 of phlebotomine sand fly vectors and exclusively as intracellular amastigote inside mammalian  
55 host phagocytic cells. Thus, *Leishmania* parasites are adapted to these two drastically different  
56 environments. From a molecular point of view, *Leishmania*, as other trypanosomatids, is unique  
57 in the Eukaryota domain (Adl et al., 2012). This includes the genomic organization in long  
58 polycistronic units, the near absence of transcription initiation regulation by RNA polymerase II  
59 promoters with gene expression regulation almost exclusively through post-  
60 transcriptional mechanisms, and its remarkable genomic plasticity (Clayton, 2019; Reis-Cunha  
61 et al., 2017). The *Leishmania* genome is generally considered to be diploid, although all  
62 *Leishmania* genomes analyzed hitherto display aneuploidy affecting at least one chromosome,  
63 i.e., a polysomy in Chr31. Moreover, high levels of ‘average’ aneuploidy (average will be used  
64 throughout this paper for features derived from bulk analyses of population of cells) affecting  
65 other chromosomes are commonly found by bulk genome sequencing (BGS) of in vitro cultured  
66 promastigotes (Downing et al., 2011; Rogers et al., 2011). This average aneuploidy is highly  
67 dynamic and changes when cultivated parasite populations are exposed to different  
68 environments such as the vector, the vertebrate host or in response to drug pressure (Dumetz

69 et al., 2017; Shaw et al., 2016; Ubeda et al., 2008). In fact, changes in average aneuploidy  
70 pattern and not variation in nucleotide sequence are the first genomic modifications  
71 observed at populational level during the course of experimental selection of drug resistance  
72 (Dumetz et al., 2018; Shaw et al., 2016). Given that these alterations in average somies are  
73 reflected in the average amount of corresponding transcripts, and to a certain degree, of  
74 proteins, it has been proposed that aneuploidy allows *Leishmania* to adapt by means of rapid  
75 changes in gene dosage (Barja et al., 2017; Cuypers, 2018; Dumetz et al., 2017).

76 *Leishmania* parasites exhibit a remarkable cellular heterogeneity in the form of mosaic  
77 aneuploidy, where individual daughter cells originating from a single parent (i.e., a clonal  
78 population) may display distinct somies (Lachaud et al., 2014; Sterkers et al., 2011). The full  
79 extent of mosaic aneuploidy in *Leishmania* and its dynamics during adaptation to new  
80 environment remains largely unexplored due to technological limitations. The only estimation  
81 of karyotype heterogeneity was based on the FISH studies of a small set of chromosomes, where  
82 it was speculated that thousands of karyotypes may co-exist in a clonal population of  
83 *Leishmania* promastigotes (Sterkers et al., 2011). Mosaicism was proposed to provide a source  
84 of functional diversity within a population of *Leishmania* cells, through gene dosage, but also  
85 through changes in heterozygosity (Barja et al., 2017; Sterkers et al., 2012). This diversity of  
86 karyotypes would provide an adaptive potential to unpredictable environmental changes  
87 during the parasite's life cycle or drug pressure caused by patient treatment (Barja et al., 2017;  
88 Sterkers et al., 2012).

89 Here, we applied and validated for the first time a high throughput, droplet-based  
90 platform for single cell genome sequencing (SCGS) of thousands of individual *Leishmania*  
91 promastigotes. This allowed the assessment of the degree and the dynamics of the evolution  
92 of mosaic aneuploidy in two clonal populations in vitro representing different stages of  
93 adaptation to culture conditions. Based on our study, we propose that the early stages of  
94 adaptation are characterized by rapid and drastic changes in karyotypes, allowing initial  
95 establishment of highly aneuploid cells in a population of almost euploid parasites. In the next  
96 steps, the existing highly aneuploid karyotypes further evolve through gradual and moderate  
97 changes in somies resulting in a population of aneuploid cells displaying closely related  
98 karyotypes. Our findings strongly support the hypothesis that mosaic aneuploidy is a  
99 constitutive feature of *Leishmania* parasites, representing a unique source of functional  
100 diversity.

101 **Materials and Methods**

102 **Parasites**

103 In the present paper we use the terms population, strain and clone as defined in the  
104 supplementary text. *L. donovani* promastigotes were maintained at 26 °C in HOMEM medium  
105 (Gibco, ThermoFisher) supplemented with 20% Fetal Bovine Serum, with regular passages done  
106 every 7 days at 1/25 dilutions. The clones BPK282 cl4 and BPK081 cl8 were derived from two  
107 strains adapted to culture: MHOM/NP/02/BPK282/0 and MHOM/NP/02/BPK081/0 (Imamura  
108 et al., 2016). These clones were submitted to SCGS at 21 (~126 generations) and 7 passages  
109 (~56 generations) after cloning respectively (supp. fig.1). Four strains were mixed to create an  
110 artificial ‘super-mosaic’ population of cells (further called super-mosaic): BPK475  
111 (MHOM/NP/09/BPK475/9), BPK498 (MHOM/NP/09/BPK498/0), BPK506  
112 (MHOM/NP/09/BPK506/0) and HU3 (MHOM/ET/67/HU3). They were kept in vitro for several  
113 passages after isolation from patients (respectively 41, 60, 47 and more than 24) and mixed at  
114 equivalent ratio just before preparation for SCGS.

115 **Single-cell suspensions preparation and sequencing**

116 Promastigotes at early stationary phase (day 5) were harvested by centrifugation at 1000 rcf  
117 for 5 min, washed twice with PBS 1X (calcium and magnesium-free) + 0.04% BSA, diluted to  
118  $5 \times 10^6$  parasites/mL and passed through a 5 µm strainer to remove clumps of cells. After  
119 straining, volume was adjusted with PBS 1X + 0.04% BSA to achieve a final concentration of  
120  $3 \times 10^6$  parasites/mL. The absence of remaining cell doublets or clumps in the cell suspension  
121 was confirmed by microscopy. Cell viability was estimated by flow cytometry (BD FACSVerse™)  
122 using the NucRed™ Dead 647 probe (Life technologies™) following the recommendations of  
123 the manufacturer and in all samples was estimated as higher than 95%. SCGS was performed  
124 using the Chromium™ single-cell CNV solution (scCNV) from 10X Genomics™. To target an  
125 average of 2000 sequenced cells per sample, 4.2 µL of the cell suspensions were used as input,  
126 and cell encapsulation, barcoding, whole genome amplification and library preparation were  
127 performed following manufacturer’s recommendations. Sequencing of the libraries was done  
128 with an Illumina NovaSeq™ SP platform with 2x150 bp reads.

129 **Single-Cell Somy estimation**

130 Details about the bioinformatics analysis for somy values determination are provided in the  
131 supplementary material. In summary, sequence reads were associated to each sequenced cell

132 based on their barcodes and mapped to a customized version of the reference *L. donovani*  
133 genome LdBPv2 (Dumetz et al., 2017) using the Cell Ranger DNA™ software (10X Genomics).  
134 The matrix generated by the software with the number of mapped reads per 20kb bins was  
135 used as input to a custom script written in R (R Core Team, 2013). In this script, bins with outlier  
136 values were excluded, and the mean normalized read depth (MNRD) of each chromosome was  
137 calculated for each cell. Cells displaying a high intra-chromosomal variation were removed from  
138 downstream analysis. In order to establish the baseline ploidy of each cell, the MNRD values  
139 were multiplied by the scale factor (Sc), defined for each cell as the lowest number between 1.8  
140 and 5 that leads to the shortest distance to integers when all MNRD values are multiplied by it.  
141 The MNRD values multiplied by Sc are referred here as ‘raw somies’. To convert the raw somies  
142 (continuous) into integer copy numbers (discrete), a univariate gaussian mixture-model was  
143 built for each chromosome by an expectation-maximization algorithm based on the distribution  
144 of the raw somy values between all cells of the same sample using the Mixtools package  
145 (Benaglia et al., 2009). For each possible integer somy, a gaussian mixture-model was generated  
146 and each raw somy value was assigned to the rounded mean of the gaussian to which it has  
147 higher probability of belonging to.

#### 148 **Karyotype identification and network analysis**

149 A karyotype was defined as the combination of integer somies of all chromosomes in a cell.  
150 Karyotypes were numerically named according to their frequency in the sequenced population.  
151 To generate the network representing the dissimilarities between the karyotypes, a pairwise  
152 distance matrix was built based on the number of different chromosomes between all  
153 karyotypes in a sample, and used to create a randomized minimum spanning tree with 100  
154 randomizations, using the Pegas R package (Paradis, 2018, 2010). The network visualization was  
155 made with the visNetwork package (Almende B.V. et al., 2019).

#### 156 **Doublet detection**

157 The relative fraction of doublets within the super mosaic population has been estimated  
158 based on the high number of SNPs found in the HU3 strain when compared to the *L. donovani*  
159 reference genome. The three other strains in the super mosaic only show a limited number of  
160 SNPs in contrast. Potential doublets were identified by looking for mixture of both SNP profiles  
161 (HU3 and non-HU3) in assumed single-cell data. This approach was applied using an in-house

162 developed algorithm and the Demuxlet algorithm (Kang et al., 2018), both approaches leading  
163 to identical results (see Supplementary Text).

164 **DNA probes and fluorescence in situ hybridization**

165 DNA probes were either cosmid (L549 specific of chromosome 1) or BAC (LB00822 and  
166 LB00273 for chromosomes 5 and 22 respectively) clones that were kindly provided by Peter  
167 Myler (Seattle Biomedical Research Institute) and Christiane Hertz-Fowler (Sanger Centre). DNA  
168 was prepared using Qiagen Large-Construct Kit and labelled with tetramethyl-rhodamine-5-  
169 dUTP (Roche Applied Sciences) by using the Nick Translation Mix (Roche Applied Sciences)  
170 according to manufacturer instructions. *Leishmania* cells were fixed in 4% paraformaldehyde  
171 then air-dried on microscope immunofluorescence slides, dehydrated in serial ethanol baths  
172 (50–100%) and incubated in NP40 0.1 % for 5 min at RT. Around 100 ng of labelled DNA probe  
173 was diluted in hybridization solution containing 50% formamide, 10% dextran sulfate, 2× SSPE,  
174 250 µg.mL<sup>-1</sup> salmon sperm DNA. Slides were hybridized with a heat-denatured DNA probe  
175 under a sealed rubber frame at 94 °C for 2 min and then overnight at 37 °C and sequentially  
176 washed in 50% formamide/2× SSC at 37 °C for 30 min, 2× SSC at 50 °C for 10 min, 2× SSC at 60  
177 °C for 10 min, 4× SSC at room temperature. Finally, slides were mounted in Vectashield (Vector  
178 Laboratories) with DAPI. Fluorescence was visualized using appropriate filters on a Zeiss  
179 Axioplan 2 microscope with a 100× objective. Digital images were captured using a  
180 Photometrics CoolSnap CCD camera (Roper Scientific) and processed with MetaView (Universal  
181 Imaging). Z-Stack image acquisitions (15 planes of 0.25 µm) were systematically performed for  
182 each cell analyzed using a Piezo controller, allowing to view the nucleus in all planes and to  
183 count the total number of labelled chromosomes. Around 200 cells [187-228] were analyzed  
184 per chromosome.

185 **Bulk Genome Sequencing (BGS)**

186 Genomic DNA from the BPK282 cl4 and BPK081 cl8 clones was extracted in bulk using the  
187 QIAamp™ DNA Mini kit (Qiagen) following manufacturer's recommendations. PCR-free whole  
188 genome sequencing was performed on the Illumina NovaSeq platform using 2x150 bp paired  
189 reads. Reads are mapped to the reference genome *L. donovani* LdBPKv2 (available at  
190 <ftp://ftp.sanger.ac.uk/pub/project/pathogens/Leishmania/donovani/LdBPKPAC2016beta/>)  
191 using BWA (version 0.7.17) with seed length set to 100 (Li and Durbin, 2009). Only properly  
192 paired reads with a mapping quality higher than 30 were selected using SAMtools (Li et al.,

193 2009). Duplicates reads were removed using the RemoveDuplicates command in the Picard  
194 software (<http://broadinstitute.github.io/picard/>). The average somy values were calculated as  
195 described previously (Downing et al., 2011), by dividing the median sequencing depth of a  
196 chromosome by the overall median sequencing depth over all chromosomes, and multiplying  
197 this ratio by 2. These values were used to define an average karyotype for the sequenced  
198 population of cells (Kp).

199 **Gene Ontology analysis and in silico screening for small RNA**

200 Gene Ontology (GO) classes were obtained from TriTrypDB release 49 (Aslett et al., 2009).  
201 As the genome sequence stored on TriTrypDB does not correspond with the reference genome  
202 used in this work, the GO annotation was obtained by mapping back all genes to our reference  
203 genome using BlastP (Altschul et al., 1997). Clustering of the different chromosomes based on  
204 their assigned GO classes was performed using the prcomp command in R.

205 The Rfam (Kalvari et al., 2021) database version 14.4 was used to screen the *L. donovani*  
206 BPK282 reference genome using the cmscan algorithm as implemented in Infernal (Nawrocki  
207 and Eddy, 2013) using default parameters and setting the search space parameter to 64.

208 **Results**

209 **High throughput single-cell genome sequencing as a reliable tool to explore karyotype**  
210 **heterogeneity in *Leishmania* populations**

211 We applied high throughput single-cell genome sequencing (SCGS) to address mosaic  
212 aneuploidy in promastigotes of two *Leishmania* clones differing substantially in average  
213 aneuploidy (referred here as the ‘average populational karyotype’, or Kp) as revealed by Bulk  
214 Genome Sequencing (BGS): (i) BPK282 cl4, an aneuploid clone showing 7 chromosomes with an  
215 average trisomy apart from the usual average tetrasomy in Chr31 and (ii) BPK081 cl8, showing  
216 an average disomy for all chromosomes except Chr31 (average tetrasomic); for simplicity, we  
217 will call BPK081 cl8 the ‘diploid’ clone. First analyses of the SCGS data were made with the Cell  
218 Ranger DNA™ pipeline. Although the software was developed for mammalian genomes, which  
219 are up to 2 orders of magnitude larger than *Leishmania*’s nuclear genome, it allowed detecting  
220 (i) aneuploidy, (ii) mosaicism and (iii) large intrachromosomal CNVs, as, for instance, the H- and  
221 M- amplicons (Downing et al., 2011) in Chr23 and Chr36 respectively (Suppl. fig 2). However,  
222 technical artifacts were noticed especially in BPK081 cl8, where the software’s GC bias  
223 correction algorithm, designed for the mammalian genome which display a lower average GC  
224 content compared to *Leishmania*, ended up overcompensating the depth of bins with high GC  
225 content (Suppl. fig 2). Because of that and given our main goal of using SCGS to study mosaic  
226 aneuploidy, we built our own analytical bioinformatic pipeline with a higher emphasis on  
227 estimating whole chromosomes copy numbers rather than local CNVs (Suppl. fig 3).

228 We evaluated the SCGS method and our analytical pipeline by first addressing their ability to  
229 explore karyotype heterogeneity among *Leishmania* cells of clones BPK282 cl4 and BPK081 cl8.  
230 Using our analytical pipeline, we identified 208 different karyotypes among the 1516 filtered  
231 cells of BPK282 cl4 and 117 karyotypes among the 2378 filtered cells of BPK081 cl8 (fig.1 A-B,  
232 Suppl. fig 5 A-B). Moreover, the cumulative SCGS profile of each clone was consistent with their  
233 respective Kp (fig. 1A and 1B, left panel). Notably, Chr13, which displays a non-integer average  
234 somy value (2.26) in the Kp of BPK282 cl4, was found as disomic and trisomic at relatively high  
235 proportions in the SCGS, resulting in a similar cumulative somy (2.34). As expected, the vast  
236 majority of cells in BPK081 cl8 displayed an almost diploid karyotype, with only Chr31 displaying  
237 a tetrasomy as expected. Small subpopulations of cells displaying highly aneuploid karyotypes  
238 were also observed in BPK081 cl8 (discussed below).

239 Mosaic aneuploidy in *Leishmania* has been studied so far with fluorescence in situ  
240 hybridization (FISH), the only alternative method available hitherto to estimate the copy  
241 number of some chromosomes in individual *Leishmania* cells. As a mutual benchmark of both  
242 FISH and SCGS methods, we submitted cells from both BPK282 cl4 and BPK081 cl8 to FISH to  
243 estimate the copy number of chromosomes 1, 5 and 22 and to compare the obtained results  
244 with the values observed in our SCGS data (fig. 1C). Overall, for each chromosome, the same  
245 predominant somy was observed with both methods, even when the predominant somy was  
246 different between clones. For instance, FISH and SCGS report Chr5 in BPK282 cl4 as trisomic in  
247 most cells, while it is reported as mainly disomic in BPK081 cl8 also by both techniques. Most  
248 discrepancies between the proportions obtained by both methods are within the 10% error  
249 margin previously estimated for FISH (Sterkers et al., 2011 and unpublished results). The main  
250 exception is Chr5 in BPK282, which is estimated as trisomic in 93% of the cells with SCGS and  
251 66% with FISH. However, SCGS reports proportions which are more consistent with the average  
252 somy values obtained by the BGS analysis of each clone. For instance, the weighted mean  
253 between somy values obtained with SCGS for Chr5 in BPK282 cl4 results in an average somy of  
254 2.95, which is very similar to the average somy value obtained by BGS (2.97), whereas with FISH,  
255 the average somy is lower (2.66), suggesting that the proportions observed with SCGS are more  
256 accurate.

257 We executed an extra experiment to evaluate the performance of SCGS in dealing with  
258 populations with highly heterogeneous karyotypes. In this experiment, a 'super-mosaic'  
259 population was generated by mixing 4 different *L. donovani* strains that display very distinct  
260 Kp's (Imamura et al., 2016), into a single SCGS run. A total of 1900 promastigotes were  
261 individually sequenced, of which, 1636 remained after data filtering. This 'super mosaic'  
262 population displayed a high aneuploidy diversity: 388 identified karyotypes in total. As  
263 expected, the 1636 promastigotes formed four distinct clusters based on their integer somy  
264 values, with discrete differences in the aneuploidy patterns between each cluster (fig. 1D). Since  
265 one of the strains (HU3) used in this super mosaic is phylogenetically distant from the other 3  
266 strains (BPK475, BPK498 and BPK506), we could distinguish HU3 promastigotes from the others  
267 based on their SNP profiles. Interestingly, all HU3 cells were grouped together in cluster C (fig.  
268 1D – orange lines in the annotation bar), suggesting that the discrete karyotypic differences  
269 between the major clusters reflect differences among the aneuploidy profiles of the four  
270 strains, so that each cluster likely represents one of the strains. Thus, this experiment

271 demonstrates that SCGS is effective in distinguishing karyotypes even in very complex  
272 populations.

273 The 'super-mosaic' population was also used to estimate the frequency of doublets, i.e, the  
274 inclusion in a single droplet of two or more cells sharing the same 10X barcode. Based on the  
275 SNP profile of the HU3 line, each dataset with the same barcode containing either none of the  
276 HU3-specific SNPs (< 5% of the SNPs), or almost all of the HU3-specific SNPs (> 95% of the SNPs)  
277 were defined as singlets, while doublets contained a mixture of HU3-specific SNPs and positions  
278 resembling the reference genome. Using this approach, from the 293 cells that were predicted  
279 as HU3 based on their SNP profile (including cells removed from karyotype estimation), 21 were  
280 predicted as doublets (fig. 1D; purple lines in the annotation bar), with a detection rate of SNPs  
281 varying between 14% and 58%. Since doublets formed by two HU3 cells would still be defined  
282 as a singlet and given that HU3 cells correspond to 15,4% of the population, we assumed that  
283 the 21 detected HU3+BPK doublets correspond to 84,6% of the total number of doublets  
284 containing an HU3 cell. Thus, we estimate that there are ~4 (the extra 15,4%) additional  
285 HU3+HU3 doublets, resulting in a total of 25 doublets. Extrapolating this fraction of 25 out of  
286 293 HU3 cells to the whole single-cell population would correspond to a relative fraction of  
287 doublets of 8,53%, a frequency which is higher than anticipated for mammal cells according to  
288 the manufacturer's guidelines (~1,4%). From the 21 detected doublets, 3 were originally  
289 removed from karyotype estimation due to high intra-chromosomal variation, and 6 displayed  
290 a karyotype that was also found in other cells. However, 11 karyotypes were exclusively found  
291 in one of the detected doublets (fig. 1E), indicating that a fraction of the low-occurrence  
292 karyotypes might be artifacts due to doublets.

293

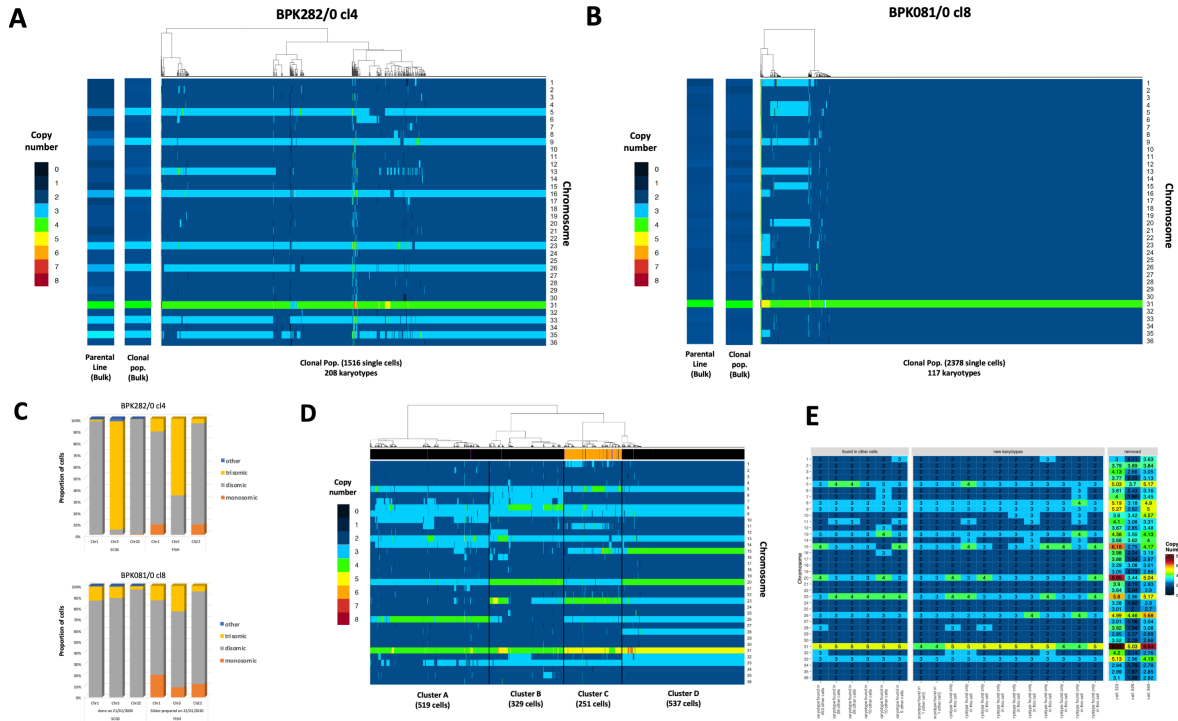


**Figure 1** - Mosaic aneuploidy in BPK282 cl4 and BPK081 cl8 clones revealed by SCGS and validation of the method. **A-B.** Heat maps displaying the copy number of all 36 chromosomes of promastigotes from BPK282 cl4 (A) or BPK081 cl8 (B) clones (main panels). Each column represents a single parasite. The number of sequenced promastigotes and karyotypes found in each sample is described in the x axis. In each panel, two insets display the Kp of the clonal population used in the SCGS and their respective parental strain. **C.** Comparison between FISH and SCGS. The proportion of cells displaying monosomy, disomy or trisomy for chromosomes 1, 5 and 22 in each method is represented. **D.** Heat map displaying the karyotypes of the promastigotes from 4 different strains mixed in a single SCGS run. Cells were hierarchically clustered according to their karyotypes, forming 4 major clusters. The number of cells in each cluster is indicated in the x axis. The bar at the top of the heatmap indicate if the SNP profile of the cell correspond to a BPK strain (black), a HU3 strain (orange) or a doublet (purple). **E.** Karyotypes of cells marked as doublets. The number of other cells displaying the same karyotype as the doublet is indicated in the x axis labels. Cells that were removed from analysis due to high intra-chromosomal variation and therefore did not have their somy values converted to integers are separated in the right panel, displaying their raw somy values instead. The integer somy values (left panels) or the raw somy values (right panel) are numerically indicated inside the heat map.

295      **BPK282 and BPK081 cells display different patterns of karyotype evolution during clonal  
296      expansion**

297      After validating the SCGS method for resolving complex karyotype heterogeneity in  
298      *Leishmania*, we returned to the data of BPK282 cl4 and BPK081 cl8 to characterize the  
299      karyotypes that are present in each clone. In BPK282 cl4, the most frequent karyotypes were  
300      very similar to each other, diverging by copy number changes in 1 to 3 chromosomes when  
301      compared to the most frequent karyotype (kar1 – fig. 2A). In BPK081 cl8, however, the nearly  
302      diploid kar1, which was present in 82% of the cells, and the 2 next most abundant karyotypes  
303      showed very different aneuploidy profiles, diverging by copy numbers of 8 to 10 chromosomes  
304      (fig. 2B). In addition, in both clones, the most frequent karyotype (kar1) is similar to the Kp of  
305      the respective parent strain from which each clone was derived (fig. 1 A-B, left panel),  
306      suggesting that, in each clone, kar1 corresponds to the karyotype of the founder cell, and thus,  
307      the other karyotypes of each population arose from their respective kar1.

308      To develop a hypothesis of the karyotype evolution during expansion of both BPK282 cl4 and  
309      BPK081 cl8 populations, we built a dissimilarity network based on the number of chromosomes  
310      with different copy numbers between each karyotype found in each population (fig. 2C). Both  
311      populations of cells are at different stages of expansion (about 126 and 56 generations since  
312      cloning, respectively), but we observe in each of them a proportionally comparable number of  
313      somy changes events (steps in the network): (i) for BPK282 cl4, 514 steps/126 generations/1516  
314      sequenced cells = 0.0027 and (ii) for BPK081 cl8, 260 steps/56 generations/2378 sequenced  
315      cells = 0.002. However, distinct patterns are observed between both clones. In BPK282 cl4, the  
316      most frequent karyotypes (black nodes) are linked to each other by somy changes in only single  
317      chromosomes (black lines). Assuming kar1 as the founder of this population, almost every  
318      frequent karyotype can be traced back to it through cumulative single copy number alterations.  
319      In contrast, the network of BPK081 cl8 shows a very distinct pattern (fig. 2C). Here, the 3 most  
320      frequent karyotypes are distant from one another and lack single-step intermediates between  
321      them.

322

323

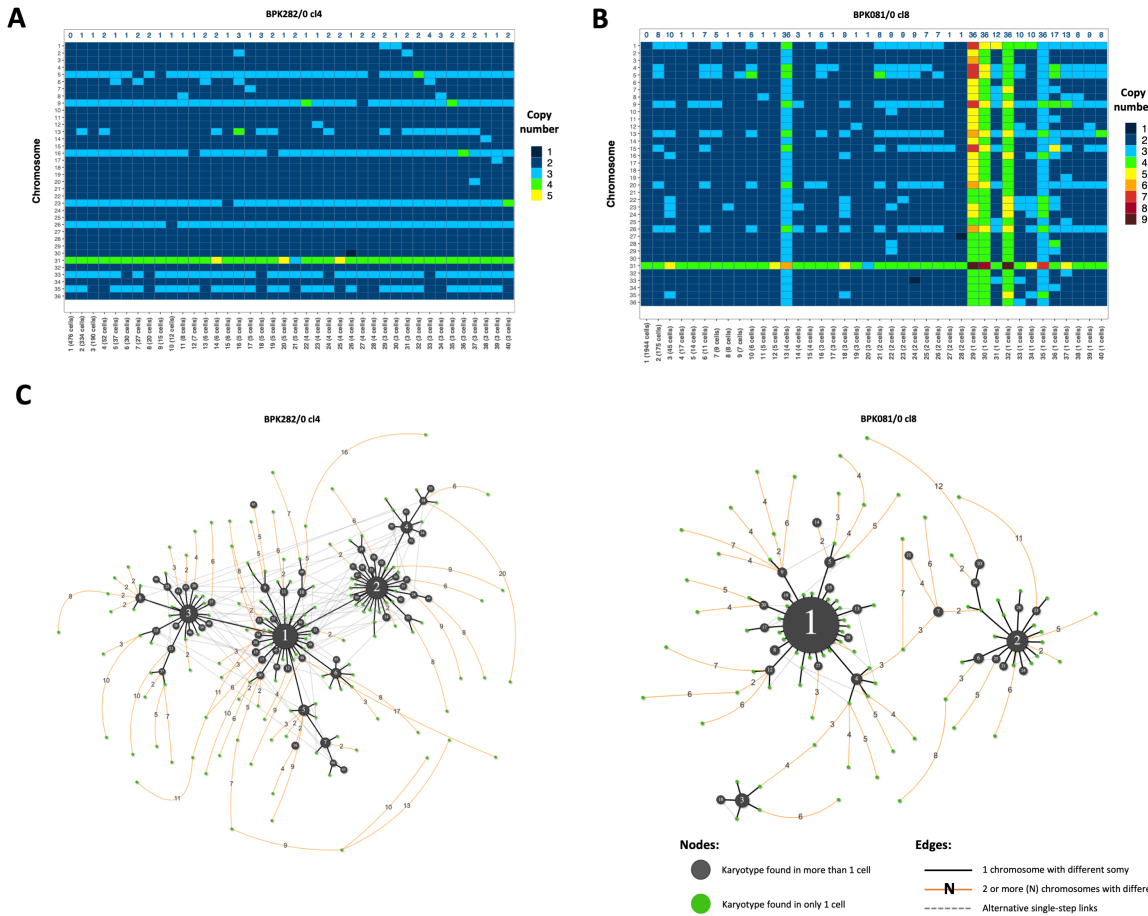


**Figure 2 - BPK282 cl4 and BPK081 cl8 display different profiles in the dissimilarity relationship between karyotypes. A-B.** Heat map depicting the 40 most frequent karyotypes in BPK282 cl4 (A) and BPK081 cl8 (B) clones. The blue numbers in the top indicate the total number of chromosomes with a different somy compared to kar1. **C.** Network representing the dissimilarity relationship between karyotypes in each clone. Black nodes represent karyotypes found in more than one cell, with their size proportional to the number of cells. Green nodes indicate karyotypes which occur only once. Black lines link two karyotypes which diverge by a somy difference in a single chromosome, while orange lines link karyotypes diverging by two or more chromosomes with different somy, with the number of divergent chromosomes indicated in the edge. Dashed grey lines show alternative links between karyotypes with a single somy divergency. Polyploid karyotypes were not included in the networks.

324

325 **Selective forces restrict high frequencies of polysomies to a specific group of chromosomes**

326 We and others have demonstrated that high frequencies of polysomies were restricted to a  
327 specific subset of chromosomes when comparing the Kp's of 204 *L. donovani* strains previously  
328 analyzed by BGS (Barja et al., 2017; Imamura et al., 2016). To address if the same applies to  
329 single *Leishmania* cells, we created a diverse artificial population by randomly selecting and  
330 merging the data of equal numbers of single cells from BPK282 cl4 and BPK081 cl8 as well as  
331 from each cluster of the super mosaic, assuming each cluster represents one of the mixed  
332 strains. In this artificial population, we observed that at least 16 chromosomes are consistently  
333 disomic in the vast majority of cells in a clone/strain-independent manner (fig. 3A). All these  
334 chromosomes also show an average disomy in the Kp of most of the 204 strains mentioned  
335 above (supp. fig. 7A-B). Conversely, apart from the usually tetrasomic Chr31, 8 chromosomes  
336 (Chr5, Chr8, Chr9, Chr13, Chr20, Chr23, Chr26 and Chr33) are found with 3 or more copies in  
337 most cells of BPK282 cl4 and BPK081 cl8, again fitting with previous observations made on the  
338 204 *L. donovani* strains (Barja et al., 2017; Imamura et al., 2016). However, it is unclear whether  
339 (i) the disparity in the frequency of polysomies between chromosomes is due to intrinsic  
340 differences in the chances of overamplification of each chromosome along the expansion of the  
341 population (some chromosomes being specifically 'unstable') or (ii) if every chromosome has  
342 the potential to become polysomic but the expansion of polysomies in a population is  
343 determined by selective pressures. To address this, we revisited the karyotype network of each  
344 population (including the 'super-mosaic' – supp. fig. 7C), to investigate which were the  
345 chromosomes that were more prone to somy alterations in the rare karyotypes (i.e., karyotypes  
346 occurring in only a single cell), compared to the common karyotypes (i.e., karyotypes occurring  
347 in 2 or more cells) (fig. 3B). As expected, the 16 chromosomes which are predominantly found  
348 as disomic display little, if any, alteration events in their copy numbers in the common  
349 karyotypes. However, between the rare karyotypes, all chromosomes are susceptible to somy  
350 alterations with relatively similar frequencies, although polysomy-prone chromosomes still  
351 display a higher alteration frequency (p-value < 0.0001 – supp. fig. 7D). These observations  
352 suggest that the capacity for aneuploidy is not restricted to a specific group of 'unstable'  
353 chromosomes.

354 We also investigated the role of the synchronous fluctuation in the copy number of multiple  
355 chromosomes in determining the abundance of karyotypes. For that, we estimated Pearson  
356 correlations between the copy number of chromosomes across equal numbers of cells from all

357 clones/strains sequenced here (supp. fig. 7E). Between the 8 polysomy-prone chromosomes  
358 and among the cells with common karyotypes, we observed numerous and relatively strong  
359 correlations, with the strongest correlations occurring between Chr5 and Chr9, and Chr8 and  
360 Chr20 (fig. 3C). On the other hand, between cells with rare karyotypes, there were fewer and  
361 in general weaker correlations (fig. 3D). These observations suggest that the expansion of  
362 polysomies in a population happens in an interdependent manner between chromosomes.

363 **Functional characterization of the polysomy-prone chromosomes**

364 In order to investigate potential features specific to the polysomy-prone chromosomes that  
365 could be related to their higher frequency of polysomies, we first applied an unsupervised Gene  
366 Ontology (GO) analysis to look for enrichment of biological functions in the polysomy-prone  
367 chromosomes. However, no obvious relationships between chromosomal gene content and  
368 prevalence of polysomies could be found (supp. fig. 8A). We then tried a supervised approach.  
369 Since highly aneuploid karyotypes are more frequently observed in in vitro promastigotes than  
370 in amastigotes, we reasoned that the amplification of the polysomic-prone chromosomes might  
371 affect pathways related to the promastigote stage. Thus, we selected enriched GO classes which  
372 were obtained from a previously published study in which we studied differential expression  
373 between promastigote and amastigote cell cultures (Dumetz et al., 2017). The distribution of  
374 the corresponding genes on the polysomy-prone chromosomes was compared to the  
375 distribution on chromosomes with a stable disomy. However, this approach also did not  
376 disclose biological functions located on the amplified chromosomes (supp. fig. 8B). Alternatively  
377 to GO analysis, we finally performed an in silico scan for small non-coding RNAs to investigate  
378 their distribution throughout the *L. donovani* genome. This suggested an enrichment of small  
379 RNAs in some of the polysomy-prone chromosomes, especially small nucleolar RNAs (snoRNAs  
380 - fig. 3E). A significant number of hits for snoRNAs are mapped to Chr5, Chr26 and Chr33, which  
381 are among the chromosomes with the most frequent polysomies, as well as Chr35, which is  
382 trisomic in the majority of BPK282 cl4 cells and is also trisomic in the Kp of several *L. donovani*  
383 strains (Imamura et al., 2016). Although preliminary, this observation suggests a potential  
384 relationship between the snoRNAs content of a chromosome and its prevalence of polysomies  
385 in cultivated promastigotes.

386

387

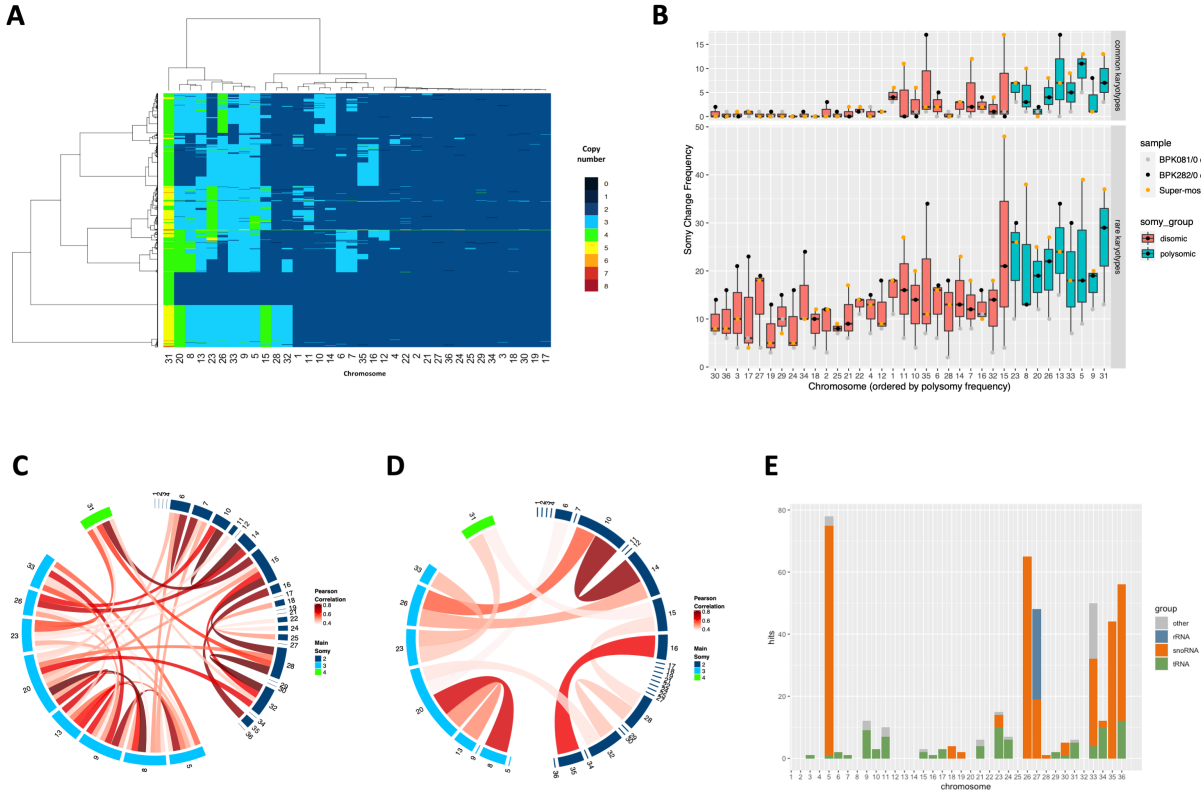


**Figure 3 - High frequencies of polysomies are restricted to a group of chromosomes.** **A.** Heat map depicting the copy number of the 36 chromosomes across promastigotes from different clones/strains. Here, 251 promastigotes of each cluster of the mixed sample and from BPK282 cl4 and BPK081 cl8 are represented. Chromosomes are hierarchically clustered based on their somy values. **B.** Boxplot indicating the number of somy change events for each chromosome among the common karyotypes (found in 2 or more cells – top panel) or the rare karyotypes (found in only one cell - bottom) in the 3 samples submitted to SCGS. **C-D.** Chord diagrams representing the Pearson correlation between the somies of all chromosomes among cells displaying the common karyotypes (**C**) or the rare karyotypes (**D**). Only correlations higher than 0.4 and with p.value lower than 0.05 are represented. **E.** Distribution of small non-coding RNAs across *L. donovani* genome. Ribosomal RNAs (rRNA), small nucleolar RNAs (snoRNAs) and transporter RNAs (tRNAs) were identified based on the Rfam database.

389 **SCGS reveals particular karyotypes among rare single cells**

390 As shown above, kar2 and kar3 of BPK081 cl8 show a baseline diploidy, i.e., the majority of  
391 chromosomes are disomic, with 8 to 10 trisomic chromosomes and tetrasomy or even a  
392 pentasomy for Chr 31. However, we found in the same population 4 cells displaying a  
393 karyotype (kar13) with an aneuploidy profile similar to kar2, but with all chromosomes showing  
394 one extra copy (two extra copies for Chr31 - fig. 2B); thus in kar11, baseline somies are trisomic,  
395 8 chromosomes (the same as kar2) are tetrasomic and Chr31 is hexasomic, constituting a  
396 triploid karyotype (see supplementary text for details on how cells ploidies are determined).  
397 Similarly, at least 1 cell showed another karyotype (kar35) with baseline triploidy and  
398 aneuploidy on the same chromosomes as kar3 (fig. 2B) . Tetraploid karyotypes were also  
399 observed among BPK081 cl8 cells, but it is not possible to rule out that these are in fact doublets  
400 between two 2n cells with different karyotypes. Noteworthy, tetraploid karyotypes were not  
401 found in BPK282 cl4 and the only 3 cells identified with a potential baseline triploidy exhibited  
402 an aneuploidy pattern very distinctive from any other karyotype in that population (supp. fig.  
403 6). Moreover, within the BPK282 cl4 and BPK081 cl8 populations, we also observed rare cells  
404 displaying chromosomes with an estimated somy of 0 (nullisomy). The bam file of these cells  
405 showed that no reads were mapping to these chromosomes, suggesting that in these cells,  
406 these chromosomes were absent (fig. 4A). Nullisomic chromosomes were found in all the  
407 populations sequenced here: among which, 4 in BPK081 cl8 (0,15% of the sequenced cells) and  
408 15 from BPK282 cl4 (0,88%). Moreover, the aneuploidy profile of these nullisomic cells was not  
409 similar to any other karyotype identified in each sample (fig. 4B). Partial chromosome deletions  
410 were also observed, as for instance in Chr13 and Chr36 of the cell 688 from BPK282 cl4, in the  
411 Chr36 of the cell 266 from BPK081 cl8.

412

413

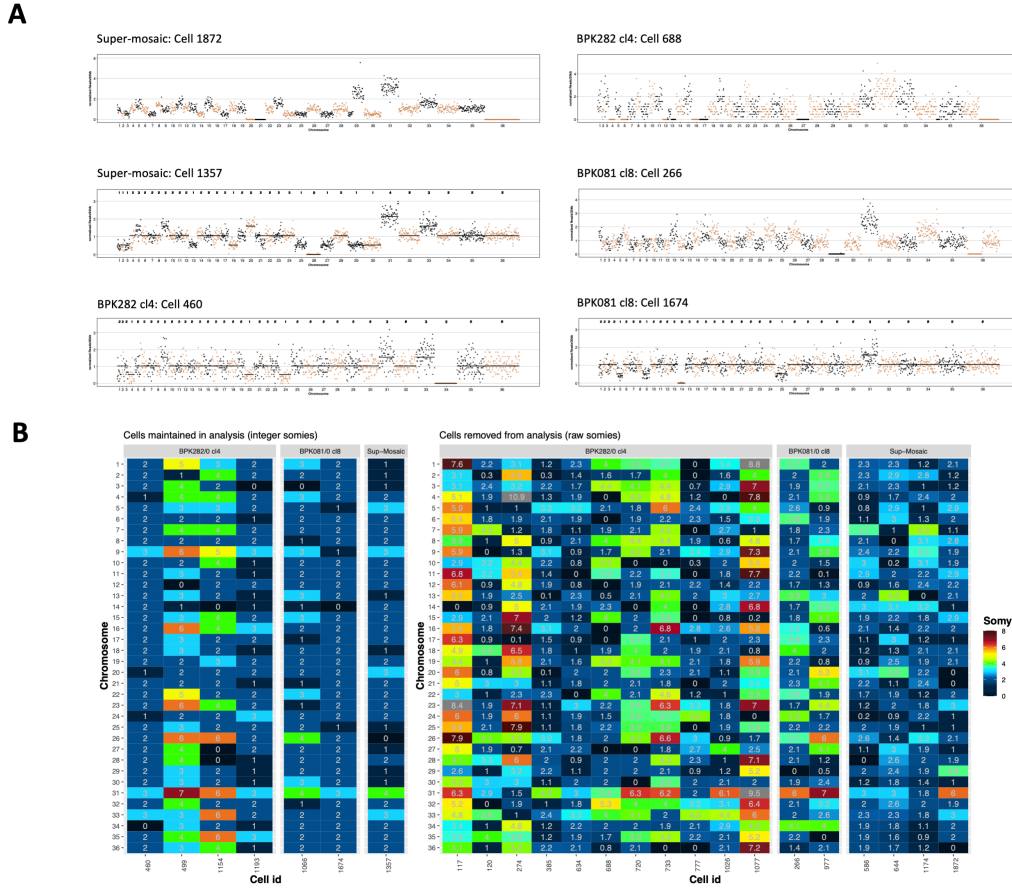


**Figure 4 - Cells with nullisomic chromosomes. A.** Example of cells displaying one or more nullisomic chromosomes. The dots represent the normalized read depth of each 20kb bin. The integer somy values calculated for each cell are depicted in the top part of each box for cells that were not excluded from analysis. A black line shows the integer somy values divided by the cell's scale factor (Sc) for comparison. **B.** Karyotype of all cells with at least one nullisomic chromosome identified in our SCGS data. Cells that were removed from analysis and therefore did not have their somy values converted to integers are separated in the right panel, displaying their raw somy values instead.

414

415

416

417 **Discussion**

418 Cellular heterogeneity is increasingly implicated as one of the major sources of adaptative  
419 potential for unicellular pathogens (Bagamery et al., 2020; Seco-Hidalgo et al., 2015). We  
420 explored here a specific manifestation of this phenomenon, i.e., mosaic aneuploidy, in a unique  
421 model, *Leishmania*. By applying a high throughput SCGS method, we could determine for the  
422 first time the complete karyotype of thousands of individual *Leishmania* cells from two distinct  
423 clonal populations in vitro. We found a high level of mosaic aneuploidy, affecting essentially the  
424 same, limited subset of chromosomes. We explored the evolution of mosaicism in both  
425 populations, starting from two distinct founder karyotypes, one nearly euploid and another  
426 highly aneuploid. We highlighted the adaptive potential of mosaic aneuploidy for unicellular  
427 organisms such as *Leishmania*, living in rapidly varying environments.

428 The present SCGS study allowed us to evaluate and extend hypotheses on mosaic aneuploidy  
429 in *Leishmania* previously based on FISH measurements (Sterkers et al., 2012, 2011). Although  
430 some divergencies were observed here between FISH and SCGS, our data are in agreement with  
431 most predictions. Accordingly, mosaic aneuploidy was confirmed in all populations sequenced  
432 here, and karyotypes frequency distributions, in particular for BPK282/0 cl4 clone (208  
433 karyotypes among 1516 cells), were similar to the distribution predicted with FISH data  
434 obtained for 7 chromosomes of a long-term cultivated *Leishmania major* population (~250  
435 karyotypes in ~2000 cells - Sterkers et al., 2012 – fig. 4). In BPK081/0 cl8, proportionally fewer  
436 karyotypes were identified compared to BPK282/0 cl4, which might be a consequence of either  
437 a reduced tendency of the founder diploid karyotype to somy alterations and/or due to the fact  
438 this clone was at an earlier stage of expansion in vitro (~56 generations, compared to the ~126  
439 generations in BPK282). Indeed, when normalizing the number of karyotypes, similar values  
440 were observed for both clones: respectively  $10\text{exp}^{-4}$  and  $9\text{exp}^{-4}$  new  
441 karyotypes/generation/sequenced cell.

442 Our SCGS data, however, do not corroborate the previous assumptions that all chromosomes  
443 are found with at least two somy states (Sterkers et al., 2012, 2011), as high levels of somy  
444 variation were restricted to a subset of chromosomes in our experimental conditions. We also  
445 observed a higher tendency of FISH to report trisomies and monosomies in chromosomes which  
446 were defined by SCGS as mostly disomic in almost all cells of BPK282/0 cl4 and BPK081/0 cl8  
447 clones, as chr01 and chr22. This discrepancy is likely due to accuracy limitations in FISH.

448 The SCGS data reported here also allowed us to draw some hypothesis regarding the origin  
449 and evolution of mosaic aneuploidy in vitro. We have previously demonstrated that intracellular  
450 amastigotes sequenced directly from patient samples usually display a diploid Kp similar to the  
451 Kp of the BPK081 cl8 clone, although variations in somies were observed in some samples  
452 (Domagalska et al., 2019). However, when these amastigotes were isolated from patients or  
453 experimental animals and transformed to promastigotes in vitro, in most cases their Kps  
454 progressively evolve towards highly aneuploid profiles (Domagalska et al., 2019; Dumetz et al.,  
455 2017; Giovanni Bussotti, a et al., 2018). Thus, the 2 clones here studied provide complementary  
456 models to understand the dynamics of the emergence of mosaic aneuploidy in vitro; BPK081/0  
457 cl8 which founder karyotype had the diploid profile, representing an early stage of adaptation  
458 to culture; and BPK282/0 cl4, which founder karyotype was already highly aneuploid (likely  
459 kar1), representing later stages.

460 In the BPK081 cl8, a minority of highly aneuploid subpopulations were observed, contrasting  
461 with the the founder diploid karyotype (kar1), indicating that at early stages of clonal expansion  
462 in culture, the evolution of mosaicism starts with drastic changes in karyotypes, in this case the  
463 observed changes in somy of 8 to 10 chromosomes leading to highly aneuploid cells (kar2 and  
464 kar3). These drastic changes in somies could occur through cumulative small steps, i.e., somy  
465 alterations in single chromosomes at each cell division, followed by fixation and further  
466 expansion of the fittest aneuploidies and loss of intermediate links between these karyotypes  
467 during clonal evolution. Alternatively, kar2 and kar3 in BPK081 cl8 may have originated  
468 independently from kar1 by simultaneous amplifications of multiple chromosomes. However,  
469 the presence of potentially triploid cells which resemble kar2 and kar3 opens other possibilities.  
470 On one hand, polyploidization has been demonstrated as an important mechanism in yeasts for  
471 quickly generating multiple and highly discrepant aneuploid karyotypes from a single parent  
472 through assorted mis-segregation of chromosomes during downstream cell divisions (Gerstein  
473 et al., 2015). In case a similar mechanism occurs in *Leishmania*, these 3n karyotypes found in  
474 BPK081 cl8 could represent an intermediate step between whole genome polyploidization  
475 event and reversion to aneuploid kar2 and kar3. On the other hand, 3n karyotypes could be  
476 reminiscent of hybridization, which was recently shown to occur in vitro (Louradour et al.,  
477 2020); the common observation of 3n karyotypes in *Leishmania* after hybridization in sand flies  
478 supports this hypothesis (Akopyants et al., 2009; Inbar et al., 2019, 2013; Romano et al., 2014).

479 Surrounding the 3 major karyotypes in the network of BPK081/0 cl8, other minor karyotypes  
480 with single somy alterations are observed, suggesting that once a successful karyotype expands,  
481 small variations of it are continuously generated by small changes in somies. This pattern is  
482 more evident in the karyotype network of BPK282/0 cl4, where almost all karyotypes which are  
483 found in at least 2 cells are at one somy change distance from another karyotype, suggesting  
484 that these karyotypes were also continuously generated by cumulative steps of small somy  
485 alterations. Accordingly, the founder karyotype of this clone (likely kar1) was already highly  
486 aneuploid and well adapted to culture, as the parent population from which BPK282/0 cl4 was  
487 isolated was already in culture for 21 passages (supp. fig. 1).

488 Highly aneuploidy Kps are observed in most in vitro cultured *Leishmania* promastigotes  
489 analysed so far by BGS (Franssen et al., 2020; Imamura et al., 2016; Van den Broeck et al., 2020).  
490 This usually affects a specific group of chromosomes, largely overlapping with the 8 polysomy-  
491 prone chromosomes described here. The early amplifications reproducibly observed in the Kp  
492 of parasite populations in transition from in vivo to in vitro (Domagalska et al., 2019; Giovanni  
493 Bussotti, a et al., 2018) suggest an adaptative role for specific polysomies in adaptation to  
494 culture. However, the mechanisms that determine which chromosomes are amplified are still  
495 poorly understood.

496 By investigating which chromosomes were more prone to somy alterations in rare and  
497 common karyotypes, we gathered evidence suggesting that all chromosomes can be  
498 stochastically amplified during population expansion, potentially at different rates, but selective  
499 forces likely dictate the higher frequency of polysomies observed in some chromosomes.  
500 Changes in the average chromosome copy numbers of cell populations are directly reflected in  
501 the average amount of transcripts encoded by the genes present on these chromosomes (Barja  
502 et al., 2017; Dumetz et al., 2017) and to a certain degree also affect the average amount of  
503 certain proteins (Cuypers, 2018). Consequently, aneuploidy might lead to dosage imbalances  
504 between the product of genes located in chromosomes that display different somies. The  
505 frequently observed co-modulation of multiple chromosomes – estimated with Pearson  
506 correlations here and across the Kp of 204 *L. donovani* isolates as previously described (Barja et  
507 al., 2017) – might reflect a dynamic compensation mechanism that reduces these imbalances  
508 and at the same time increases the dosage of key genes. Our GO analyses did not reveal any  
509 enrichment of biological functions in the (co-)amplified chromosomes. However, we observed  
510 an enrichment of snoRNA genes in some of the polysomy-prone chromosomes, accordingly

511 Chr05, Chr26, Chr33 and Chr35. This class of small RNAs is involved in the extensive processing  
512 of ribosomal RNA (rRNA) characteristic of trypanosomatids, directly affecting ribosomal  
513 biosynthesis and ultimately translation, both increased in cultured promastigotes (Jara et al.,  
514 2017; Martínez-Calvillo et al., 2019). Amplification of these chromosomes as seen in many cells  
515 in vitro might ultimately boost the translation capacity of the cells due to a consequent higher  
516 abundance of snoRNAs. At the time of submission of the present article, a very recent study  
517 supporting and further addressing this hypothesis was pre-printed (Piel et al., 2021).

518 The high diversity of karyotypes identified in both models here described is in agreement  
519 with the idea of mosaic aneuploidy being a constitutive feature in *Leishmania* (Lachaud et al.,  
520 2014). The generation of karyotypic heterogeneity represents a source of functional diversity,  
521 due to variations in genes dosage (Dumetz et al., 2017), and it is also expected to facilitate the  
522 removal of detrimental mutations and the fixation of beneficial haplotypes (Barja et al., 2017;  
523 Sterkers et al., 2012). Although in a given environment some very different karyotypes might  
524 be limited to low frequencies, they may provide to the population a major (pre-)adaptation  
525 potential to unpredictable environmental changes, such as a change of host or drug pressure  
526 associated to chemotherapy (Dumetz et al., 2018, 2017; Shaw et al., 2016, 2020). Time-lapse  
527 SCGS studies of populations of parasites during clonal expansion under stable or varying  
528 environments are needed to test this pre-adaptation hypothesis. Combining SCGS with single-  
529 cell transcriptomics could also allow to understand better the impact of gene dosage imbalance  
530 on transcription with a single-cell resolution. Thus, high throughput single-cell sequencing  
531 methods represent a remarkable tool to understand key aspects of *Leishmania* biology and  
532 adaptability.

533

534 **Acknowledgements**

535 We thank Prof. Dr. Thierry Backeljau for comments on the manuscript. This study received  
536 financial support from the Flemish Ministry of Science and Innovation (SOFI Grant MADLEI) and  
537 the Flemish Fund for Scientific Research (FWO, post-doctoral grant to FVdB). A.Y. was recipient  
538 of a grant from the Agence Nationale de la Recherche (ANR) within the frame of the  
539 “Investissements d’avenir” programme (ANR 11-LABX-0024-01 “ParaFrap”).

540 **Author contributions**

541 All authors have approved the submitted version of this manuscript and have agreed both to  
542 be personally accountable for their own contributions and to ensure that questions related to  
543 the accuracy or integrity of any part of the work are appropriately investigated and resolved.  
544 This work was conceived and designed by GN, JCD & MAD. Data were acquired and analyzed by  
545 GN, PM, HI, IM, NK, AY, YS, JCD and MAD. Data interpretation was made by GN, PM, FVdB, YS,  
546 JCD and MAD. Paper was drafted by GN, PM, JCD and MAD and substantively revised by HI,  
547 FVdB and YS.

548

549 **References**

550 Adl SM, Simpson AG, Lane CE, Lukeš J, Bass D, Bowser SS, Brown M, Burki F, Dunthorn M, Hampl  
551 V, Heiss A, Hoppenrath M, Lara E, Lynn DH, Mcmanus H, Mitchell EAD, Mozley-Stanridge SE,  
552 Parfrey LW, Pawlowski J, Rueckert S, Shadwick L, Schoch C, Smirnov A, Spiegel FW, Ca SA. 2012.  
553 The revised classification of eukaryotes HHS Public Access. *J Eukaryot Microbiol Microbiol*  
554 **59**:429–493. doi:10.1111/j.1550-7408.2012.00644.x.The

555 Akopyants NS, Kimblin N, Secundino N, Patrick R, Peters N, Lawyer P, Dobson DE, Beverley SM,  
556 Sacks DL. 2009. Demonstration of Genetic Exchange During Cyclical Development of  
557 &lt;em&gt;Leishmania&lt;/em&gt; in the Sand Fly Vector. *Science (80- )* **324**:265 LP – 268.  
558 doi:10.1126/science.1169464

559 Almende B.V., Thieurmel B, Robert T. 2019. visNetwork: Network Visualization using “vis.js”  
560 Library.

561 Altschul SF, Madden TL, Schäffer AA, Zhang J, Zhang Z, Miller W, Lipman DJ. 1997. Gapped BLAST  
562 and PSI-BLAST: a new generation of protein database search programs. *Nucleic Acids Res*  
563 **25**:3389–3402. doi:10.1093/nar/25.17.3389

564 Aslett M, Aurrecoechea C, Berriman M, Brestelli J, Brunk BP, Carrington M, Depledge DP, Fischer  
565 S, Gajria B, Gao X, Gardner MJ, Gingle A, Grant G, Harb OS, Heiges M, Hertz-Fowler C, Houston  
566 R, Innamorato F, Iodice J, Kissinger JC, Kraemer E, Li W, Logan FJ, Miller JA, Mitra S, Myler PJ,  
567 Nayak V, Pennington C, Phan I, Pinney DF, Ramasamy G, Rogers MB, Roos DS, Ross C, Sivam D,  
568 Smith DF, Srinivasamoorthy G, Stoeckert CJ, Subramanian S, Thibodeau R, Tivey A, Treatman C,  
569 Velarde G, Wang H. 2009. TriTrypDB: A functional genomic resource for the Trypanosomatidae.  
570 *Nucleic Acids Res* **38**:457–462. doi:10.1093/nar/gkp851

571 Bagamery LE, Justman QA, Garner EC, Murray AW. 2020. A Putative Bet-Hedging Strategy  
572 Buffers Budding Yeast against Environmental Instability. *Curr Biol* 1–16.  
573 doi:10.1016/j.cub.2020.08.092

574 Barja PP, Pescher P, Bussotti G, Dumetz F, Imamura H, Kedra D, Domagalska MA, Chaumeau V,  
575 Himmelbauer H, Pages M, Sterkers Y, Dujardin J-C, Notredame C, Späth GF. 2017. Haplotype  
576 selection as an adaptive mechanism in the protozoan pathogen *Leishmania donovani*. *Nat Ecol  
577 Evol* **1**:1961–1969. doi:10.1038/s41559-017-0361-x

578 Beach RR, Ricci-Tam C, Brennan CM, Moomau CA, Hsu P hsin, Hua B, Silberman RE, Springer M,  
579 Amon A. 2017. Aneuploidy Causes Non-genetic Individuality. *Cell* **169**:229-242.e21.  
580 doi:10.1016/j.cell.2017.03.021

581 Benaglia T, Chauveau D, Hunter DR, Young D. 2009. {mixtools}: An {R} Package for Analyzing  
582 Finite Mixture Models. *J Stat Softw* **32**:1–29.

583 Clayton C. 2019. Regulation of gene expression in trypanosomatids: Living with polycistronic  
584 transcription. *Open Biol* **9**. doi:10.1098/rsob.190072

585 Cuypers B. 2018. A systems biology approach for a comprehensive understanding of molecular  
586 adaptation in *Leishmania donovani*.

587 Domagalska MA, Imamura H, Sanders M, Van den Broeck F, Bhattarai NR, Vanaerschot M, Maes  
588 I, D’Haenens E, Rai K, Rijal S, Berriman M, Cotton JA, Dujardin J-C. 2019. Genomes of *Leishmania*  
589 parasites directly sequenced from patients with visceral leishmaniasis in the Indian  
590 subcontinent. *PLoS Negl Trop Dis* **13**:e0007900. doi:10.1371/journal.pntd.0007900

591 Downing T, Imamura H, Decuypere S, Clark TG, Coombs GH, Cotton JA, Hilly JD, De Doncker S,  
592 Maes I, Mottram JC, Quail MA, Rijal S, Sanders M, Schönian G, Stark O, Sundar S, Vanaerschot  
593 M, Hertz-Fowler C, Dujardin J-C, Berriman M. 2011. Whole genome sequencing of multiple  
594 *Leishmania donovani* clinical isolates provides insights into population structure and  
595 mechanisms of drug resistance. *Genome Res* **21**:2143–2156. doi:10.1101/gr.123430.111

596 Dumetz F, Cuypers B, Imamura H, Zander D, D’Haenens E, Maes I, Domagalska MA, Clos J,  
597 Dujardin J-C, De Muylder G. 2018. Molecular Preadaptation to Antimony Resistance in  
598 *Leishmania donovani* on the Indian Subcontinent. *mSphere* **3**:e00548-17.  
599 doi:10.1128/mSphere.00548-17

600 Dumetz F, Imamura H, Sanders M, Seblova V, Myskova J, Pescher P, Vanaerschot M, Meehan  
601 CJ, Cuypers B, De Muylder G, Späth GF, Bussotti G, Vermeesch JR, Berriman M, Cotton JA, Volf  
602 P, Dujardin J-C, Domagalska MA. 2017. Modulation of aneuploidy in *leishmania donovani* during  
603 adaptation to different in vitro and in vivo environments and its impact on gene expression.  
604 *MBio* **8**:1–14. doi:10.1128/mBio.00599-17

605 Franssen SU, Durrant C, Stark O, Moser B, Downing T, Imamura H, Dujardin JC, Sanders MJ,

606 Mauricio I, Miles MA, Schnur LF, Jaffe CL, Nasereddin A, Schallig H, Yeo M, Bhattacharyya T,  
607 Alam MZ, Berriman M, Wirth T, Schönian G, Cotton JA. 2020. Global genome diversity of the  
608 *Leishmania donovani* complex. *Elife* **9**:1–44. doi:10.7554/eLife.51243

609 Gerstein AC, Fu MS, Mukaremra L, Li Z, Ormerod KL, Fraser JA, Berman J, Nielsen K. 2015.  
610 Polyploid titan cells produce haploid and aneuploid progeny to promote stress adaptation.  
611 *MBio* **6**:1–14. doi:10.1128/mBio.01340-15

612 Gilchrist C, Stelkens R. 2019. Aneuploidy in yeast: Segregation error or adaptation mechanism?  
613 *Yeast* **36**:525–539. doi:10.1002/yea.3427

614 Giovanni Bussotti, a B, Evi Gouzelou B, Mariana Côrtes Boité, c Ihcen Kherachi D, Zoubir Harrat,  
615 d Naouel Eddaikra D, Jeremy C. Mottram, e Maria Antoniou F, Vasiliki Christodoulou F, Aymen  
616 Bali, g H, Fatma Z. Guerfali, g, h Dhafer Laouini, g H, Maowia Mukhtar I, Franck Dumetz, j Jean-  
617 Claude Dujardin, j K, Despina Smirlis L, Pierre Lechat, a Pascale Pescher B, Adil El Hamouchi M,  
618 Meryem Lemrani, m Carmen Chicharro N, Ivonne Pamela Llanes-Acevedo, n Laura Botana, n  
619 Israel Cruz, n Javier Moreno, n Fakhri Jedd, h O, Karim Aoun, h O, Aïda Bouratbine, h, o Elisa  
620 Cupolillo c GFS. 2018. Leishmania Genome Dynamics during Environmental Adaptation Reveal  
621 Strain-Specific Differences in Gene Copy Number Variation, Karyotype Instability, and Telomeric  
622 Amplification. *MBio* **9**:1–18. doi:10.1128/mBio.01399-18

623 Hirakawa M, Chyou D, Huang D, Sian A, Bennett R. 2017. Parasex Generates Phenotypic  
624 Diversity and Impacts Drug Resistance and Virulence in . *Genetics* **207**:1195–1211.  
625 doi:10.1534/genetics.117.300295/-/DC1.1

626 Holland AJ, Cleveland DW. 2009. Boveri revisited: Chromosomal instability, aneuploidy and  
627 tumorigenesis. *Nat Rev Mol Cell Biol* **10**:478–487. doi:10.1038/nrm2718

628 Hu G, Wang J, Choi J, Jung WH, Liu I, Litvintseva AP, Bicanic T, Aurora R, Mitchell TG, Perfect JR,  
629 Kronstad JW. 2011. Variation in chromosome copy number influences the virulence of  
630 *Cryptococcus neoformans* and occurs in isolates from AIDS patients. *BMC Genomics* **12**.  
631 doi:10.1186/1471-2164-12-526

632 Imamura H, Downing T, van den Broeck F, Sanders MJ, Rijal S, Sundar S, Mannaert A,  
633 Vanaerschot M, Berg M, de Muylde G, Dumetz F, Cuypers B, Maes I, Domagalska MA,  
634 Decuypere S, Rai K, Uranw S, Bhattarai NR, Khanal B, Prajapati VK, Sharma S, Stark O, Schönian

635 G, de Koning HP, Settimo L, Vanhollebeke B, Roy S, Ostyn B, Boelaert M, Maes L, Berriman M,  
636 Dujardin J-C, Cotton JA. 2016. Evolutionary genomics of epidemic visceral leishmaniasis in the  
637 Indian subcontinent. *Elife* **5**:1–39. doi:10.7554/eLife.12613

638 Inbar E, Akopyants NS, Charmoy M, Romano A, Lawyer P, Elnaiem DEA, Kauffmann F, Barhoumi  
639 M, Grigg M, Owens K, Fay M, Dobson DE, Shaik J, Beverley SM, Sacks D. 2013. The Mating  
640 Competence of Geographically Diverse *Leishmania* major Strains in Their Natural and Unnatural  
641 Sand Fly Vectors. *PLoS Genet* **9**. doi:10.1371/journal.pgen.1003672

642 Inbar E, Id JS, Id SAI, Romano A, Nzelu CO, Owens K, Sanders MJ, Id DD, Id JAC, Grigg ME, Id  
643 SMB, Id DS. 2019. Whole genome sequencing of experimental hybrids supports meiosis-like  
644 sexual recombination in *Leishmania* 1–28.

645 Jara M, Berg M, Caljon G, de Muylder G, Cuypers B, Castillo D, Maes I, Orozco M del C,  
646 Vanaerschot M, Dujardin J-C, Arevalo J, Cuypers B, del Carmen Orozco M, Vanaerschot M,  
647 Dujardin J-C, Arevalo J. 2017. Macromolecular biosynthetic parameters and metabolic profile in  
648 different life stages of *Leishmania braziliensis*: Amastigotes as a functionally less active stage.  
649 *PLoS One* **12**:1–22.

650 Kalvari I, Nawrocki EP, Ontiveros-Palacios N, Argasinska J, Lamkiewicz K, Marz M, Griffiths-Jones  
651 S, Toffano-Nioche C, Gautheret D, Weinberg Z, Rivas E, Eddy SR, Finn RDD, Bateman A, Petrov  
652 AI. 2021. Rfam 14: expanded coverage of metagenomic, viral and microRNA families. *Nucleic  
653 Acids Res* **49**:D192–D200. doi:10.1093/nar/gkaa1047

654 Kang HM, Subramaniam M, Targ S, Nguyen M, Maliskova L, McCarthy E, Wan E, Wong S, Byrnes  
655 L, Lanata CM, Gate RE, Mostafavi S, Marson A, Zaitlen N, Criswell LA, Ye CJ. 2018. Multiplexed  
656 droplet single-cell RNA-sequencing using natural genetic variation. *Nat Biotechnol* **36**:89–94.  
657 doi:10.1038/nbt.4042

658 Lachaud L, Bourgeois N, Kuk N, Morelle C, Crobu L, Merlin G, Bastien P, Pagès M, Sterkers Y.  
659 2014. Constitutive mosaic aneuploidy is a unique genetic feature widespread in the *Leishmania*  
660 genus. *Microbes Infect* **16**:61–66. doi:10.1016/j.micinf.2013.09.005

661 Li H, Durbin R. 2009. Fast and accurate short read alignment with Burrows-Wheeler transform.  
662 *Bioinformatics* **25**:1754–1760. doi:10.1093/bioinformatics/btp324

663 Li H, Handsaker B, Wysoker A, Fennell T, Ruan J, Homer N, Marth G, Abecasis G, Durbin R. 2009.  
664 The Sequence Alignment/Map format and SAMtools. *Bioinformatics* **25**:2078–2079.  
665 doi:10.1093/bioinformatics/btp352

666 Louradour I, Ferreira TR, Ghosh K, Shaik J, Sacks DL. 2020. In Vitro Generation of Leishmania  
667 Hybrids. *Cell Rep* **31**:107507. doi:10.1016/j.celrep.2020.03.071

668 Mannaert A, Downing T, Imamura H, Dujardin J-C. 2012. Adaptive mechanisms in pathogens:  
669 Universal aneuploidy in Leishmania. *Trends Parasitol* **28**:370–376. doi:10.1016/j.pt.2012.06.003

670 Martínez-Calvillo S, Florencio-Martínez LE, Nepomuceno-Mejía T. 2019. Nucleolar Structure and  
671 Function in Trypanosomatid Protozoa. *Cells* **8**:421. doi:10.3390/cells8050421

672 Mulla W, Zhu J, Li R. 2014. Yeast: A simple model system to study complex phenomena of  
673 aneuploidy. *FEMS Microbiol Rev* **38**:201–212. doi:10.1111/1574-6976.12048

674 Nawrocki EP, Eddy SR. 2013. Infernal 1.1: 100-fold faster RNA homology searches.  
675 *Bioinformatics* **29**:2933–2935. doi:10.1093/bioinformatics/btt509

676 Ni M, Feretzaki M, Li W, Floyd-Averette A, Mieczkowski P, Dietrich FS, Heitman J. 2013.  
677 Unisexual and Heterosexual Meiotic Reproduction Generate Aneuploidy and Phenotypic  
678 Diversity De Novo in the Yeast *Cryptococcus neoformans*. *PLoS Biol* **11**.  
679 doi:10.1371/journal.pbio.1001653

680 Paradis E. 2018. Analysis of haplotype networks: The randomized minimum spanning tree  
681 method. *Methods Ecol Evol* **9**:1308–1317. doi:10.1111/2041-210X.12969

682 Paradis E. 2010. Pegas: An R package for population genetics with an integrated-modular  
683 approach. *Bioinformatics* **26**:419–420. doi:10.1093/bioinformatics/btp696

684 Piel L, Rajan KS, Bussotti G, Varet H, Legendre R, Douché T, Giai-gianetto Q, Chaze T, Vojtкова  
685 B. 2021. Post-transcriptional regulation of Leishmania fitness gain. *bioRxiv*.

686 R Core Team. 2013. R: A Language and Environment for Statistical Computing.

687 Reis-Cunha JL, Valdivia HO, Bartholomeu DC. 2017. Gene and Chromosomal Copy Number  
688 Variations as an Adaptive Mechanism Towards a Parasitic Lifestyle in Trypanosomatids. *Curr  
689 Genomics* **19**:87–97. doi:10.2174/1389202918666170911161311

690 Rogers MB, Hilley JD, Dickens NJ, Wilkes J, Bates PA, Depledge DP, Harris D, Her Y, Herzyk P,  
691 Imamura H, Otto TD, Sanders M, Seeger K, Dujardin J-C, Berriman M, Smith DF, Hertz-Fowler C,  
692 Mottram JC. 2011. Chromosome and gene copy number variation allow major structural change  
693 between species and strains of *Leishmania*. *Genome Res* **21**:2129–42.  
694 doi:10.1101/gr.122945.111

695 Romano A, Inbar E, Debrabant A, Charmoy M, Lawyer P, Ribeiro-Gomes F, Barhoumi M, Grigg  
696 M, Shaik J, Dobson D, Beverley SM, Sacks DL. 2014. Cross-species genetic exchange between  
697 visceral and cutaneous strains of *Leishmania* in the sand fly vector. *Proc Natl Acad Sci*  
698 **111**:16808–16813. doi:10.1073/pnas.1415109111

699 Seco-Hidalgo V, Osuna A, De Pablos LM. 2015. To bet or not to bet: Deciphering cell to cell  
700 variation in protozoan infections. *Trends Parasitol* **31**:350–356. doi:10.1016/j.pt.2015.05.004

701 Selmecki A, Forche A, Berman J. 2006. Aneuploidy and isochromosome formation in drug-  
702 resistant *Candida albicans*. *Science (80- )* **313**:367–370. doi:10.1126/science.1128242

703 Shaw C, Lonchamp J, Downing T, Imamura H, Freeman TM, Cotton JA, Sanders M, Blackburn G,  
704 Dujardin J-C, Rijal S, Khanal B, Illingworth CJR, Coombs GH, Carter KC. 2016. In vitro selection of  
705 miltefosine resistance in promastigotes of *Leishmania donovani* from Nepal: Genomic and  
706 metabolomic characterization. *Mol Microbiol* **99**:1134–1148. doi:10.1111/mmi.13291

707 Shaw CD, Imamura H, Downing T, Blackburn G, Westrop GD, Cotton JA, Berriman M, Sanders  
708 M, Rijal S, Coombs GH, Dujardin JC, Carter KC. 2020. Genomic and Metabolomic Polymorphism  
709 among Experimentally Selected Paromomycin-Resistant *Leishmania donovani* Strains.  
710 *Antimicrob Agents Chemother* **64**. doi:10.1128/AAC.00904-19

711 Siegel JJ, Amon A. 2012. New insights into the troubles of aneuploidy. *Annu Rev Cell Dev Biol*  
712 **28**:189–214. doi:10.1146/annurev-cellbio-101011-155807

713 Sterkers Y, Lachaud L, Bourgeois N, Crobu L, Bastien P, Pagès M. 2012. Novel insights into  
714 genome plasticity in Eukaryotes: Mosaic aneuploidy in *Leishmania*. *Mol Microbiol* **86**:15–23.  
715 doi:10.1111/j.1365-2958.2012.08185.x

716 Sterkers Y, Lachaud L, Crobu L, Bastien P, Pagès M. 2011. FISH analysis reveals aneuploidy and  
717 continual generation of chromosomal mosaicism in *Leishmania major*. *Cell Microbiol* **13**:274–

718 283. doi:10.1111/j.1462-5822.2010.01534.x

719 Ubeda JM, Légaré D, Raymond F, Ouameur AA, Boisvert S, Rigault P, Corbeil J, Tremblay MJ,  
720 Olivier M, Papadopoulou B, Ouellette M. 2008. Modulation of gene expression in drug resistant  
721 Leishmania is associated with gene amplification, gene deletion and chromosome aneuploidy.  
722 *Genome Biol* **9**. doi:10.1186/gb-2008-9-7-r115

723 Van den Broeck F, Savill NJ, Imamura H, Sanders M, Maes I, Cooper S, Mateus D, Jara M, Adaui  
724 V, Arevalo J, Llanos-Cuentas A, Garcia L, Cupolillo E, Miles M, Berriman M, Schnaufer A, Cotton  
725 JA, Dujardin JC. 2020. Ecological divergence and hybridization of Neotropical Leishmania  
726 parasites. *Proc Natl Acad Sci U S A* **117**:25159–25168. doi:10.1073/pnas.1920136117

727 WHO. 2020. Ending the neglect to attain the sustainable development goals: a road map for  
728 neglected tropical diseases 2021–2030: overview. World Health Organization.

729

730

731   Supplementary text to

732   **High throughput single-cell genome sequencing gives insights into the generation and**  
733   **evolution of mosaic aneuploidy in *Leishmania donovani***

734   by

735   Gabriel H. Negreira<sup>1</sup>, Pieter Monsieurs<sup>1</sup>, Hideo Imamura<sup>1</sup>, Ilse Maes<sup>1</sup>, Nada Kuk<sup>2</sup>, Akila Yagoubat<sup>2</sup>, Frederik  
736   Van den Broeck<sup>1</sup>, Yvon Sterkers<sup>2</sup>, Jean-Claude Dujardin<sup>1,3</sup>, Małgorzata A. Domagalska<sup>1</sup>

737

738   **Table of Contents**

|  |           |
|--|-----------|
| 739 <b><i>Definitions and Glossary</i></b> .....               | <b>34</b> |
| 740 <b><i>Supplementary methods</i></b> .....                  | <b>35</b> |
| 741      Single-cell DNA sequence data analysis .....          | 35        |
| 742      Doublet detection .....                               | 38        |
| 743 <b><i>Supplementary results &amp; discussion</i></b> ..... | <b>39</b> |
| 744      Sequencing statistics .....                           | 39        |
| 745 <b><i>Supplementary References</i></b> .....               | <b>41</b> |
| 746 <b><i>Supplementary Figures</i></b> .....                  | <b>42</b> |

747

748

749

750 **Definitions and Glossary**

751 In the present paper, we use the following definitions for population, strains and clones;  
752 adapted from the nomenclature of salivarian trypanosomes (Baker et al., 1978). Accordingly:

753 - A population is a group of *Leishmania* cells present at a given time in a given culture or  
754 host;

755 - A strain is a population derived by serial passage in vitro from a primary isolate (in our  
756 case, from patient samples) without any implication of homogeneity but with some degree of  
757 characterization (in our case bulk genome sequencing).

758 - A clone is derived from a strain and is a population of cells derived from a single  
759 individual presumably by binary fission.

760 Other terms are defined in the following glossary:

| Term                                 | Definition  |
|--------------------------------------|---|
| Bulk Genome Sequencing (BGS)         | Whole genome sequencing performed in a group of cells combined as a single sample.  |
| Single Cell Genome Sequencing (SCGS) | Genome sequencing performed in single cells individually.   |
| Somy                                 | The number of copies of a given chromosome in a cell.   |
| Polysomy                             | A somy higher than 2.   |
| Karyotype                            | The set of copy numbers of all chromosomes in a cell.   |
| Cell Karyotype                       | The karyotype of a cell determined by SCGS.   |
| Populational Karyotype (Kp)          | The average karyotype of a population determined by BGS.  |
| Ploidy                               | The most frequent somy in a karyotype.  |
| Euploidy                             | A condition where all chromosomes display the same somy in a cell.  |
| Aneuploidy                           | A condition where one or more chromosomes display a somy that diverges from the other chromosomes in the same cell.   |
| Mosaic Aneuploidy                    | A condition where different aneuploid karyotypes co-exist in the same population.   |
| Cell scale factor (Sc)               | The lowest number between 1.8 and 5 by which when the average normalized read depths of all chromosomes in a cell are multiplied the resulting numbers are the closest to integers as possible. |
| Raw somy                             | The average normalized read depth of a chromosome multiplied by Sc.   |
| Integer somy                         | The integer value assigned to a raw somy.   |

761 **Supplementary methods**

762 **Single-cell DNA sequence data analysis**

763 Illumina Base call files (BCL) were demultiplexed and converted to FASTQ files using the  
764 cellranger-dna mkfastq command of the CellRanger™ DNA pipeline (10X Genomics). The FASTQ  
765 files were then used as inputs to the cellranger-dna cnv command in order to associate reads  
766 to individual cells based on their 10X barcodes and to map reads to a customized version of the  
767 LdBP Kv2 *L. donovani* reference genome (available at  
768 <ftp://ftp.sanger.ac.uk/pub/project/pathogens/Leishmania/donovani/LdBP KPAC2016beta/>),  
769 where 'N's were added to the ends of chromosomes 1 to 5 to reach the 500kb minimum size  
770 allowed by the CellRanger DNA pipeline. The pipeline divides the genome into adjacent 20kb  
771 bins and outputs a CSV file containing the number of reads mapped to each bin. This file was  
772 used to estimate chromosomes copy number in a custom script written in R.

773 An overview of the steps performed by the script is shown in supp. fig. 3A. The script first  
774 removes bins with a low number of mapped reads by eliminating any bin showing an average  
775 depth of 0.5 read/cell. Then, the difference between the median number of reads of each bin  
776 and the chromosomal median is calculated. Bins with outlier values are determined using the  
777 boxplot.stats function from the R package grDevices v3.6.2. These outlier bins are removed  
778 from downstream analysis (supp. fig. 3B). This also excludes common local-CNVs found in some  
779 *L. donovani* strains, as for instance the H-Locus and the M-Locus in Chr23 and Chr36 respectively  
780 (Downing et al., 2011), present in the BPK strains/clones but absent in the HU3 strain. After  
781 removal of outlier bins, the bins depths are normalized by the cell mean and are used to  
782 estimate intrachromosomal variation (ICV). ICV is determined for each cell by dividing each  
783 chromosome in 3 segments and calculating the ratio between the segment with the highest and  
784 the segment with lowest depth. The mean of the five highest ICV values (i.e. the 5 most variable  
785 chromosomes in a cell) is assigned as its ICV-score. The distribution of ICV-scores in each sample  
786 was graphically analyzed in order to determine a threshold for exclusion of noisy cells. This  
787 threshold was defined as 2.0 for BPK282 cl4 and 1.7 for the BPK081 cl8 and the 'super-mosaic'  
788 samples.

789 The copy number of chromosomes in a cell is defined based on their normalized mean depth  
790 (NMD), i.e., the mean of the normalized depth values of the 20kb bins of a chromosome. In this  
791 sense, NMDs reflects the relative differences in copy number between chromosomes, but

792 absolute copy numbers must be inferred based on the ratios between NMDs of different  
793 chromosomes in a cell. Thus, considering that chromosomes copy numbers must be integers,  
794 the script uses an approach to determine absolute copy numbers which consists of multiplying  
795 NMDs by a scale factor which minimizes distances between the multiplied NMDs and integers.  
796 Therefore, the scale factor is defined as the lowest value between 1.8 and 5 which results to  
797 the closest approximation of NMDs to integers when they are multiplied by this factor. As the  
798 scale factor is directly affected by the ploidy of the cell, the limitation of the scale factor to  
799 values higher than 1.8 heuristically assumes that the lowest baseline ploidy of a cell is 2n. This  
800 was done to prevent that 2n cells with no odd somy value would be scaled as 1n cells.

801 In order to determine the scale factor, the script multiply the NMDs of a cell by 1000  
802 equidistant numbers between 1.8 and 5. For each multiplication, the difference between the  
803 resultant values and their closest integers is calculated for each chromosome and averaged.  
804 The value that results in the lowest average distance to integers is then assigned to the cell as  
805 its scale factor (supp. fig. 3C). In case two or more scale factors result in the same average  
806 distance to integers, the one with the lowest value is chosen.

807 Since *Leishmania* chromosomes are biased in GC content (Imamura et al., 2020), with small  
808 chromosomes (Chr1 to Chr5) displaying a higher GC content than others, amplification bias due  
809 to differences in GC content can have a negative impact in the determination of the copy  
810 number of these chromosomes. Plotting the distribution of NMD values leads to different  
811 peaks, each peak representing one of the somy values, however, the peaks of these small  
812 chromosomes with high GC content are shifted relative to the other chromosomes (supp. fig.  
813 3D upper panel). Thus, to compensate for chromosome-specific amplification and to further  
814 define the somies of the cells, the above explained scale factor are used at two levels, i.e., at  
815 population level (all cells combined) as well as at single cell level (defined for each cell). In this  
816 sense, the script first defines a single scale factor to the whole population (Sp) by which NMDs  
817 are multiplied and the distribution peak of the scaled NMDs of each chromosome is adjusted  
818 to the closest integer (supp. fig. 3D bottom panel). Then, these values are divided back by Sp  
819 and based on this output a second scale factor is defined for each cell (Sc). Thus, the NMDs of  
820 the chromosomes in a cell after bias compensation multiplied by the cell's Sc defines the 'raw  
821 somies' of the chromosomes of that cell.

822        Despite the fact that the abovementioned steps have moved the NMDs distribution closer  
823        to integer values, those values are still floating-point numbers. To determine the cells  
824        karyotypes, the raw floating-point somies are converted to integer copy numbers using  
825        Gaussian Mixture Models (GMMs). To generate a GMM for each chromosome, a vector  
826        containing all raw somy values determined for that chromosome among the filtered cells in a  
827        sample is used as input to the normalMixEM function of the mixtools R (Benaglia et al., 2009),  
828        following the defined rules bellow:

829        1) The possible integer values are defined as the number of different integers found when  
830        all values in the vector are rounded to the closest integer.

831        2) The number of components (k) is determined as the total number of possible integer  
832        values.

833        3) The ratio between means ( $\mu$ ) of k gaussians are constrained to the ratios between the  
834        possible integer values.

835        4) If for a given gaussian, less than 5% of the values are inside the interval between  $\mu-0.2$   
836         $< \mu < \mu+0.2$ , the standard deviation ( $\sigma$ ) of that gaussian is arbitrarily limited to 0.1.

837        5) At least 5 iterations must be performed before a gaussian is defined.

838        Thus, for each chromosome in a sample, a gaussian is built for each possible integer somy  
839        (supp. fig. 3E). Raw somies are then converted to the rounded  $\mu$  of the gaussian of which they  
840        have the higher probability of belonging to. Since the GMMs must be built between cells sharing  
841        the sample baseline ploidy, and as the vast majority of cells in all samples sequenced in the  
842        present study had a scale factor lower than 2.5 and consequently were considered 2n cells  
843        (supp. fig. 3F), the GMMs were applied only to 2n cells. Moreover, since the number of non-2n  
844        cells were always very low, GMMs could not be built separately for cells with other baseline  
845        ploidies. Thus, cells which baseline ploidy was different than 2 were treated differently. In this  
846        case, cells with intermediate somies, i.e, with at least one raw somy values that are at a distance  
847        greater than 0.4 from its closest integers, were considered unresolvable and were removed  
848        from downstream analysis. The reminiscent had their raw somy values simply rounded to the  
849        closest integer. Karyotypes were then defined as the concatenated set of integer somy values  
850        found in a cell.

851      **Doublet detection**

852      Two different methods were used for doublet detection, i.e. an in-house developed  
853      methodology and Demuxlet (Kang et al., 2018), both exploiting the difference in SNP profile  
854      between HU3 cells versus other cell lines.

855      The in-house developed approach uses the following methodology: 1) Homozygote SNPs for  
856      the HU3 strain are predicted based on the genome of the HU3 strain sequenced by BGS (data  
857      not shown). 2) For each of those HU3 homozygote SNPs, the occurrence of this SNP is derived  
858      for each of the single cells in the 4-strains mixture sample (further called ‘super-mosaic’). Given  
859      the low sequencing depth per cell (on average around 1x), this will report the absence or  
860      presence for each SNP. 3) For the HU3 cells in the super-mosaic, the majority of SNPs should be  
861      detected, while for the other three strains no SNPs should be detected. In case of a doublet  
862      consisting of a HU3 cell with a cell from one of the other three strains, two different scenarios  
863      can occur: If the sequencing depth is low, only the allele of one of the two cells can be predicted,  
864      while in case of a sufficient sequencing depth (at least 2x), both alleles (either the HU3 or the  
865      reference allele) can be detected, resulting in an allele frequency of 50%. In both cases, overall  
866      detection rate of the homozygote SNPs should be around 50%. In order to compensate for  
867      sequencing errors and differences in sequencing depth, libraries detecting between 10% and  
868      90% of the HU3 homozygote SNP list were classified as doublets. Homozygote SNPs where  
869      predicted based on the genome of the HU3 strain. Genetic variants were detected using the  
870      mpileup and call command of BCFtools (version 1.10.2). The view and query command of  
871      BCFtools were used to filter out genetic variants fulfilling the following conditions 1) minimum  
872      sequencing depth of 100, 2) only SNPs i.e., removing indels, 3) biallelic, 4) homozygous. In a  
873      second step, for each single cell those SNP positions are checked using the bcftools mpileup  
874      command.

875      Demuxlet was run using the default parameters with the following input: 1) the bam file  
876      returned by the Cell Ranger software, produced for the single-cell experiment with the super-  
877      mosaic, 2) a vcf file describing the two different SNP profiles, i.e., the SNP profile for HU3, and  
878      the SNP profile for the three other strains.

879 **Supplementary results & discussion**

880 **Sequencing statistics**

881 Summary of sequencing statistics is provided in table S1. The BPK282 cl4 and BPK081 cl8  
882 were sequenced with the same targeted depth (75.000 reads per cell) but BPK282 cl4 sample  
883 displayed a depth which was lower than anticipated (29.192 reads per cell). This was due to a  
884 high fraction (53.3%) of reads without a cell barcode in this sample, which according to the  
885 manufacturer indicates free floating DNA or a problem during library prep, but which unlikely  
886 affect copy number estimation. The scCNV library of the super-mosaic sample was sequenced  
887 deeper (209.000 reads per cell) to better allow the distinction between doublets. Higher  
888 coverage depths per cell were also associated with lower intra-chromosomal variation and  
889 lower frequency of intermediate somy values (supp. fig. 4A-B). This explains why sample  
890 BPK282 cl4 displayed a higher overall ICV score compared to the other samples.

891 The noisy nature of whole genome amplification ultimately leads, in some cases, to the  
892 existence of raw somy values are at similar distances from two integers. Although the  
893 conversion of raw somies into integers could be achieved by simply rounding the raw somy  
894 values to the closest integers, this could overestimate the number of karyotypes identified in a  
895 population, as the wrong determination of a somy value of a single chromosome in a single cell  
896 is sufficient to lead to a new artificial karyotype. Thus, in order to convert the raw somy values  
897 into integers, we used a more stringent approach by constructing GMMs based on the  
898 distribution of raw somy values of each chromosome among cells in a given sample. One of the  
899 consequences of using this approach is that the frequency of which an integer somy value is  
900 present in a population influences the probability of a raw somy value to be assigned to this  
901 integer. This favors that intermediate somy values are assigned to the most frequent integer  
902 somy values in the population, reducing the chances of misinterpreting an intermediate value  
903 as a new, rare integer, and consequently greatly reducing the number of artificial karyotypes  
904 caused by the misinterpretation of a somy. This is evident, for example, when comparing the  
905 number of karyotypes identified in the BPK282 cl4 sample using the GMMs (207 karyotypes)  
906 and when raw somies are just rounded to their closest integers (525 karyotypes - supp. fig. 4D).

907 Noisy data had also an impact on the scaling of the NMDs of cells into raw somies, as  
908 differences between chromosomes NMDs becomes less discrete. In the 3 samples submitted to  
909 SCGS here we noticed a higher ICV-score in a large fraction of cells which were scaled to baseline

910 ploidies different than 2 (supp. fig. 4C). These cells were removed from karyotype estimation  
911 either due to their ICR-score being above the threshold, or due to the presence of unresolvable  
912 intermediate somy values as described in the supplementary materials and methods.

913

914 **Supplementary References**

915 Baker JR, Brown KN, Godfrey DG. 1978. Proposals for the nomenclature of salivarian  
916 trypanosomes and for the maintenance of reference collections. *Bull World Health Organ*  
917 **56**:467–480.

918 Benaglia T, Chauveau D, Hunter DR, Young DS. 2009. Mixtools: An R package for analyzing finite  
919 mixture models. *J Stat Softw* **32**:1–29. doi:10.18637/jss.v032.i06

920 Downing T, Imamura H, Decuypere S, Clark TG, Coombs GH, Cotton JA, Hilly JD, De Doncker S,  
921 Maes I, Mottram JC, Quail MA, Rijal S, Sanders M, Schönian G, Stark O, Sundar S, Vanaerschot  
922 M, Hertz-Fowler C, Dujardin J-C, Berriman M. 2011. Whole genome sequencing of multiple  
923 Leishmania donovani clinical isolates provides insights into population structure and  
924 mechanisms of drug resistance. *Genome Res* **21**:2143–2156. doi:10.1101/gr.123430.111

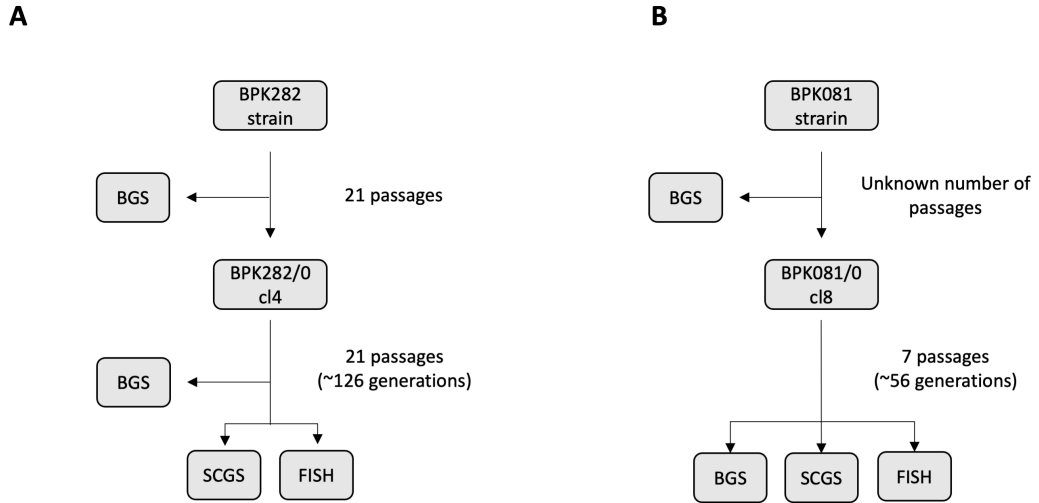
925 Imamura H, Monsieurs P, Jara M, Sanders M, Maes I, Vanaerschot M, Berriman M, Cotton JA,  
926 Dujardin JC, Domagalska MA. 2020. Evaluation of whole genome amplification and  
927 bioinformatic methods for the characterization of Leishmania genomes at a single cell level. *Sci  
928 Rep* **10**:1–13. doi:10.1038/s41598-020-71882-2

929 Kang HM, Subramaniam M, Targ S, Nguyen M, Maliskova L, McCarthy E, Wan E, Wong S, Byrnes  
930 L, Lanata CM, Gate RE, Mostafavi S, Marson A, Zaitlen N, Criswell LA, Ye CJ. 2018. Multiplexed  
931 droplet single-cell RNA-sequencing using natural genetic variation. *Nat Biotechnol* **36**:89–94.  
932 doi:10.1038/nbt.4042

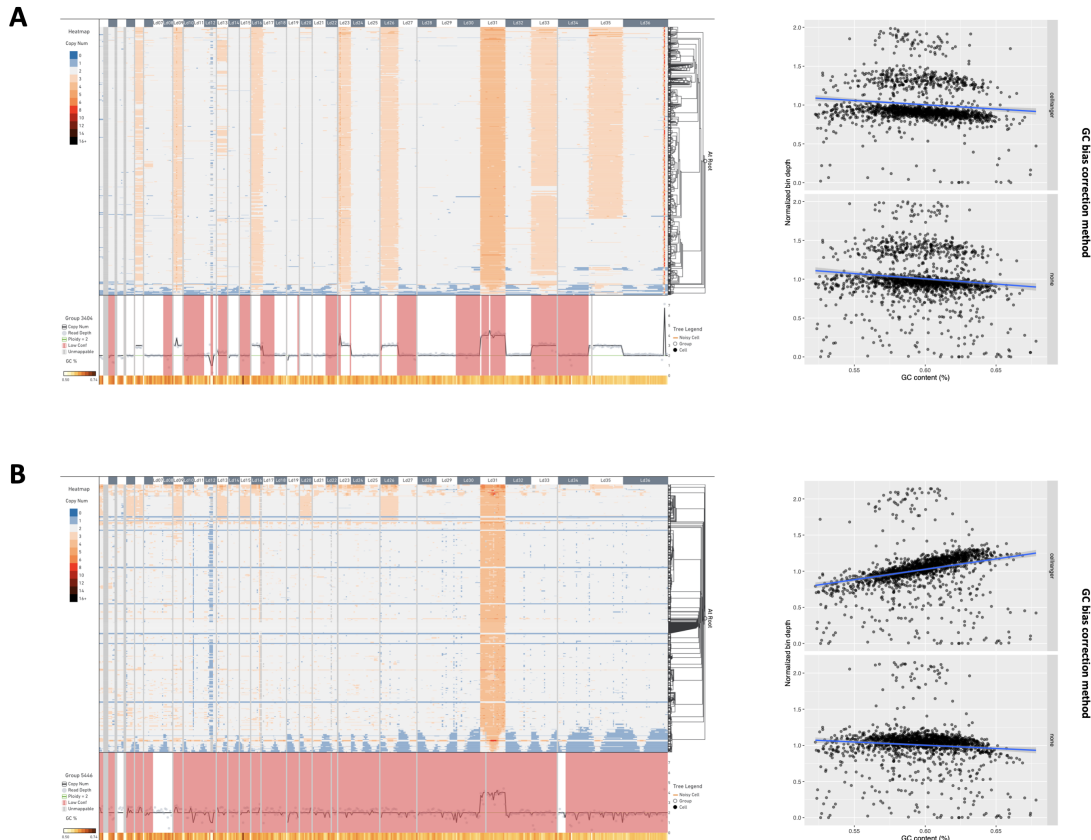
933

934

935 **Supplementary Figures**



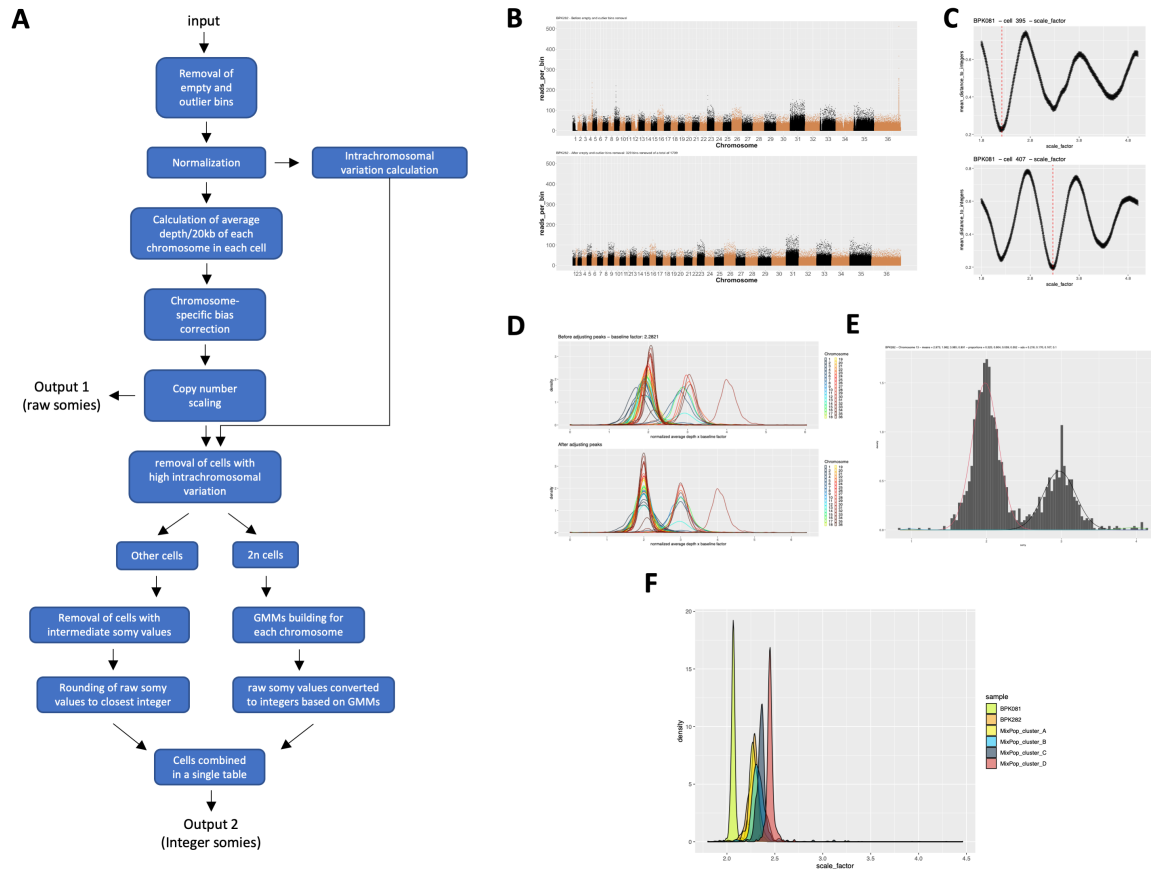
**Supplementary figure 1 – Flow chart of the two clonal populations used in the present study.** For BPK282 cl4, SCGS and FISH were performed in cultures at the same passage number. BGS was performed previously at passage 13 after cloning. For BPK081 cl8, all experiments were performed with the same culture. Number of generations is roughly estimated as  $26+((p-1)*5)$ , where  $p$  is the number of passages. This is done assuming that it takes about 26 generations to reach a total of  $\sim 7 \times 10^7$  cells starting from 1 cell, an approximation to the total number of cells usually found in a culture flask with 5mL of culture medium at the moment the first passage is done, and also assuming that each subsequent passage represents  $\sim 5$  generations.



**Supplementary figure 2** - CNV profile of BPK282 cl4 and BPK081 cl8 calculated with the Cell Ranger™ pipeline and visualized with the Loupe™ scDNA Browser software (10X Genomics). In each sample, cells (rows) are arranged in 512 clusters, the maximum number of clusters allowed by the software. CNVs (columns) are depicted in windows of 80kb. Insets on the left display the effect of the the GC bias correction algorithm of the Cell Ranger™ pipeline on the normalized read depth of bins (top) when compared to no bias correction (bottom).

936

937

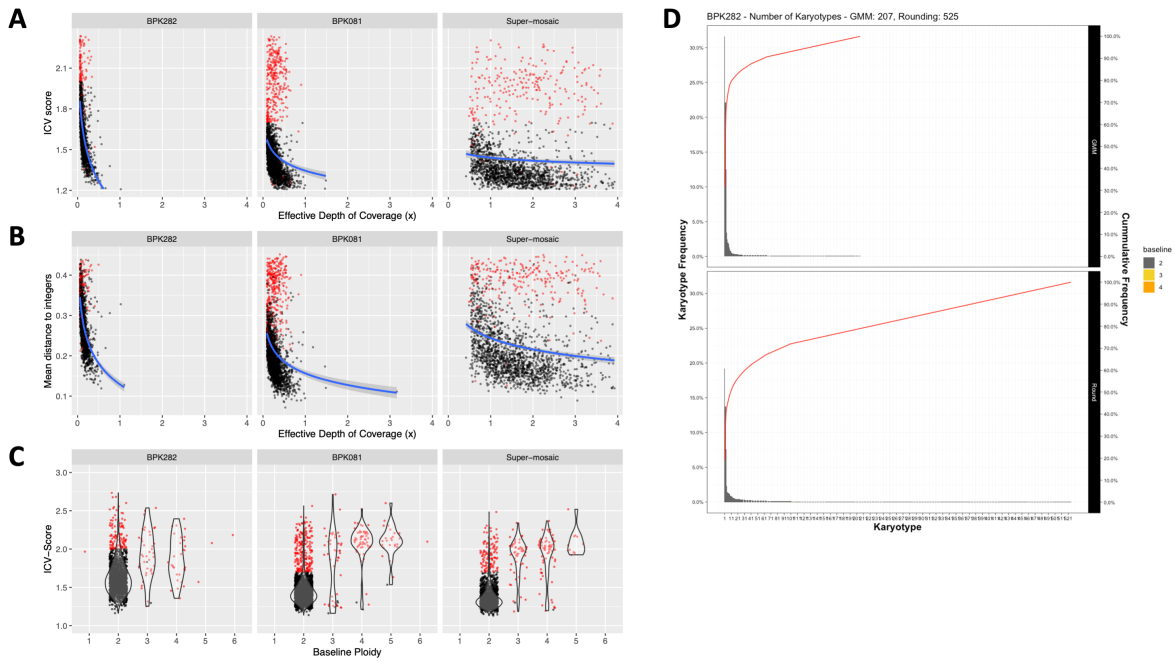


**Supplementary figure 3 - Bioinformatics pipeline for somy estimation. A.** Flow chart of the script developed to estimate chromosomes copy numbers based on their average depth/20kb bin. The input file is a matrix containing the read count of each 20kb bin for each cell. Two output files are generated, one with the raw somy values (floating points) and another with integer somy values. **B.** An example of the effect of the removal of empty and outlier bins in the BPK282 cl4 data. In this step, small intrachromosomal CNVs are also removed. **C.** Example of the determination of the scale factor for a 2N cell in the BPK081/0 cl8 sample with karyotype 2 (top panel) and a 3N cell with karyotype 13 (bottom panel). Y-axis represents the mean distance to integers when the NMDs of that cell are multiplied by a given scale\_factor (x-axis). Red dashed line denotes the scale factor value defined for that cell. **D.** An example of the chromosome-bias correction step in the BPK282 cl4 data. **E.** Example of a Gaussian Mixture Model (GMM) built for chromosome 13 in the BPK282 cl4 data. The histogram represents the distribution of raw somy values for this chromosome in this sample, while the gaussian curves represent the GMM built for it. In this step, a gaussian is built for each integer, and raw somy values are assigned to the integer corresponding to the gaussian to which they have the higher probability. **F.** Distribution of the scale factors between all cells sequenced in this study.

938

939

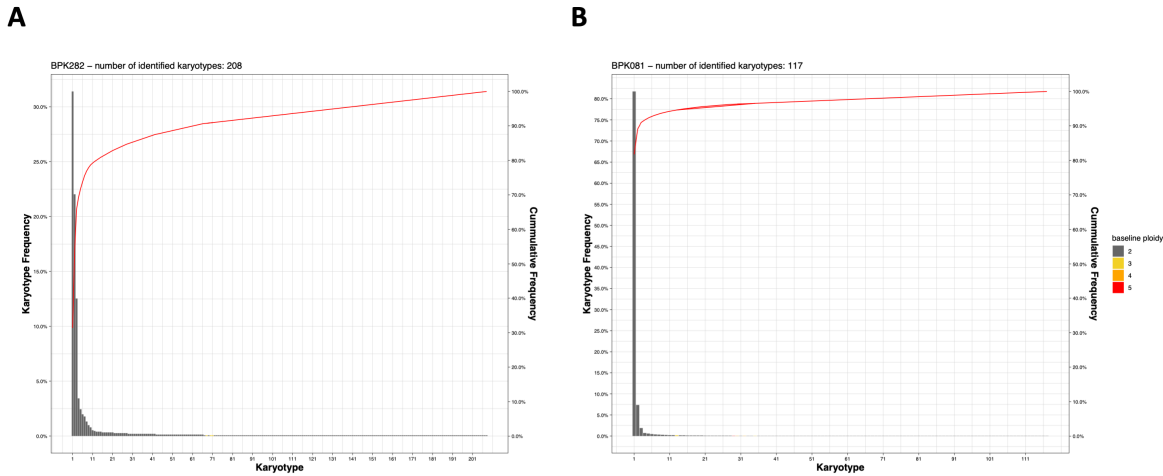
940



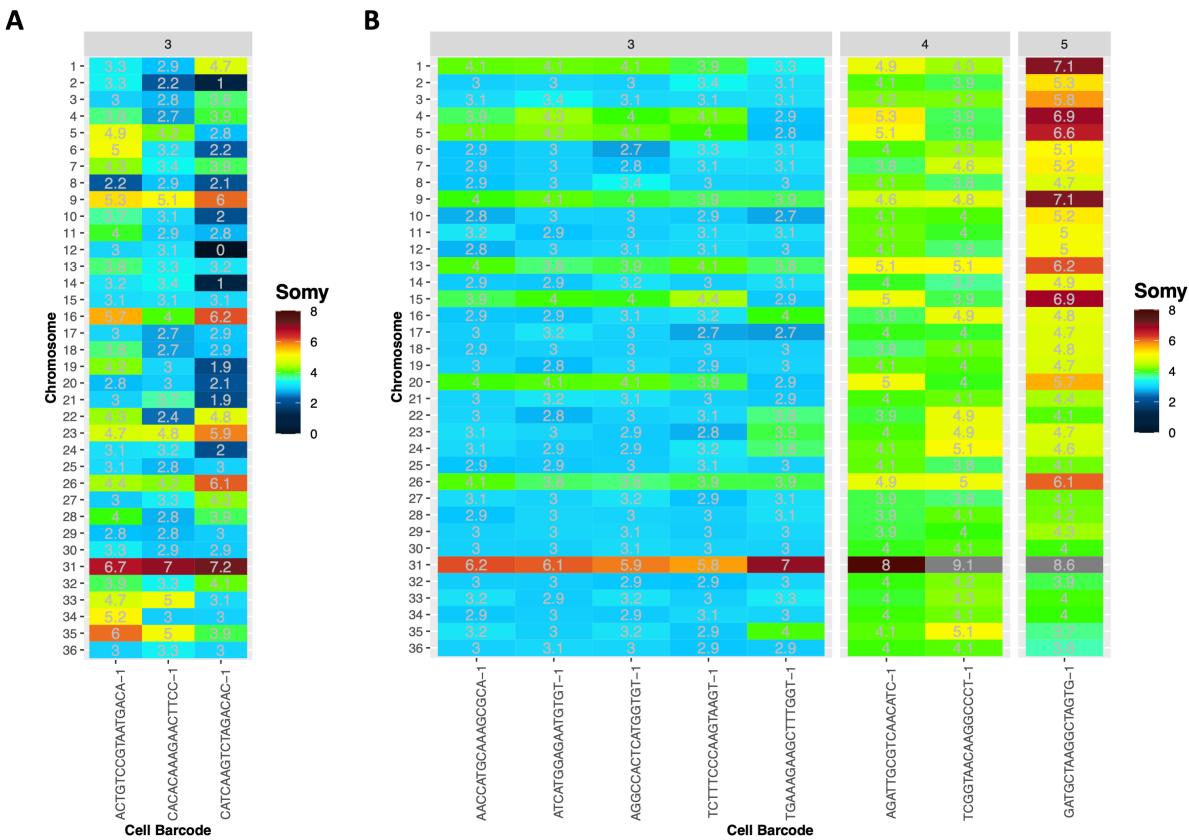
**Supplementary figure 4** – The relationship between the depth of coverage per cell and the cells ICV-score (**A**), mean distance to integers (**B**) and the relationship between the baseline ploidy defined for a cell – which is a direct consequence of the cells scale factor – and the cells ICV-score (**C**). Red dots represent cells which were removed from karyotype estimation. **D**. Comparison of the number and distribution of karyotypes identified in BPK282 when using the GMMs (top) and when raw somies are simply rounded to their closest integers (bottom).

941

942



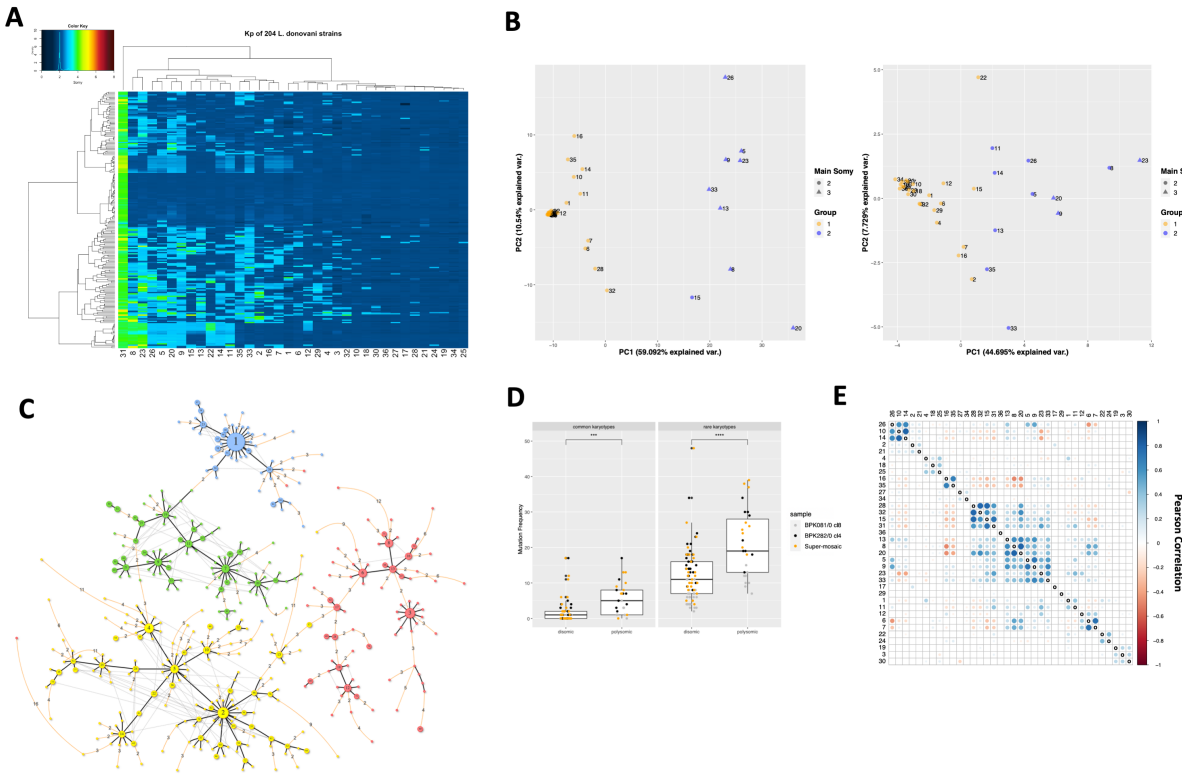
**Supplementary figure 5** - Frequency distribution of the karyotypes identified in **A.** BPK282 cl4 and **B.** BPK081 cl8 clones.

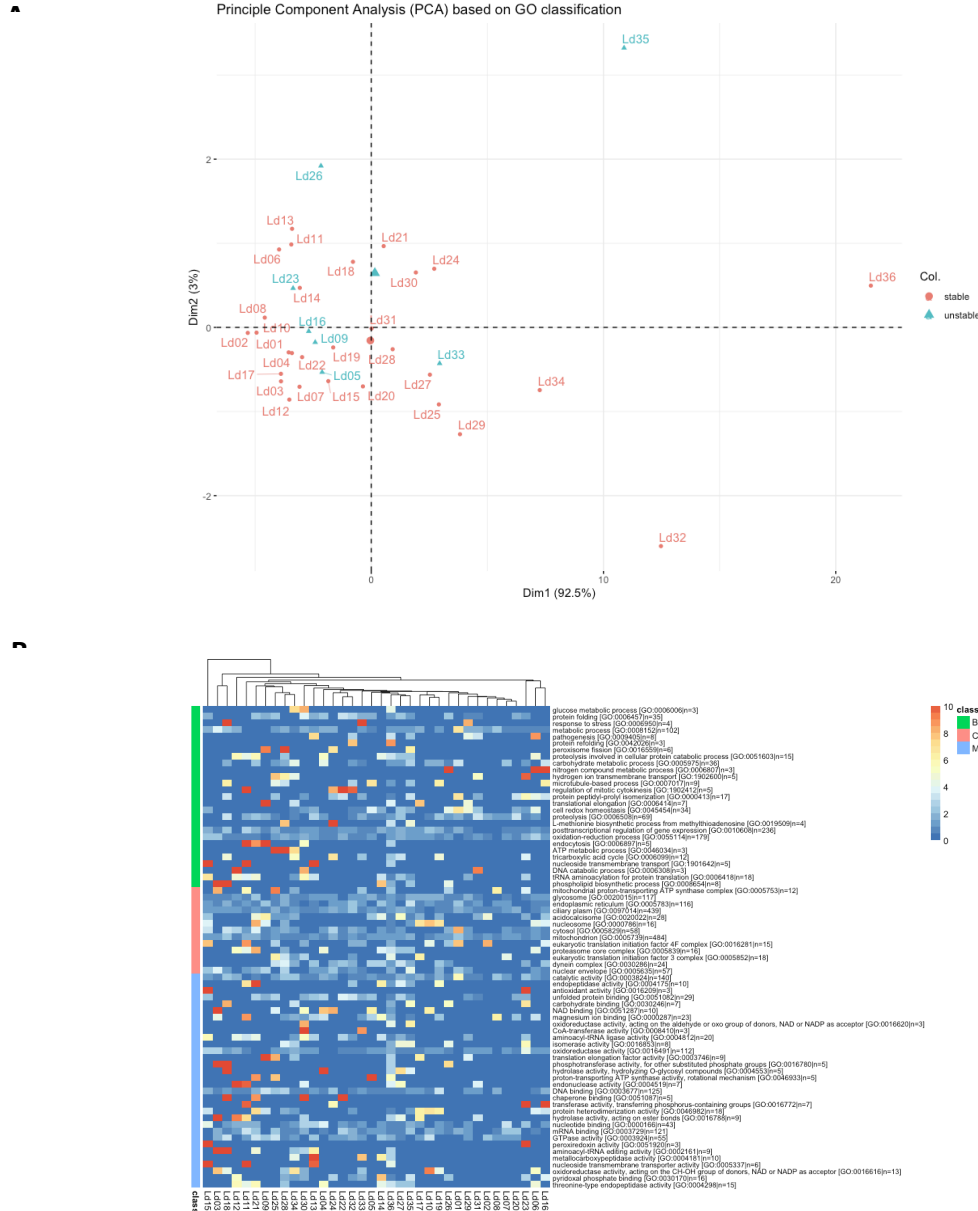


**Supplementary figure 6** - Raw somy values of potentially polyploid cells in BPK282 cl4 (**A**) and BPK081 cl8 (**B**) clones. Plots are separated by the baseline ploidy of the cells (indicated in the top).

943

944





**Supplementary figure 8 – A.** Principal component analysis (PCA) based on the Gene Ontology (GO) annotation. Based on the GO annotation provided by TriTrypDB, the percentage of each GO category (minimal category size set to 10, maximum category size set to 500), the chromosome by GO category percentage matrix is used as input for the PCA analysis. Chromosomes indicated as “stable” due to their stable disomy are indicated in red, chromosomes which showed frequent changes in ploidy level are indicated in cyan. No obvious clustering of unstable chromosomes is observed based on their GO classification **B.** Heatmap showing the ratio of the genes assigned to a GO class over the total number of genes per GO class (colour code between 0% and 10%), calculated per chromosome. The list of GO classes shown in this heatmap are significantly enriched promastigote-specific GO classes, derived based on the transcriptomics data as available in Dumetz et al. 2017, and are grouped over the three main categories i.e. Biological Process (BP), Cellular Compartment (CC) and Molecular Function (MF). No clear clustering of polysomy-prone chromosomes based on the GO classification was observed.